A&A 388, 868–888 (2002)
DOI: 10.1051/0004-6361:20020300

Astronomy & Astrophysics

Doppler Imaging of stellar magnetic fields

II. Numerical experiments

O. Kochukhov and N. Piskunov

Uppsala Astronomical Observatory, Box 515, 751 20 Uppsala, Sweden

Received 31 October 2001 / Accepted 27 February 2002

Abstract. We present numerical experiments designed to evaluate the performance of the new Magnetic Doppler Imaging (MDI) code `INVERS10`. Numerous test runs demonstrate what can be achieved with the MDI method and allow assessment of the systematic errors that can cause distortions of the maps. Our numerical experiments showed that given high-resolution observations in four Stokes parameters the code is capable of reconstructing abundance and magnetic field vector distributions simultaneously and without any prior assumptions about the magnetic field geometry. At the same time we found that in order to achieve reliable reconstruction using only circular polarization data it is necessary to impose additional constraints on the possible structure of the magnetic field. Numerical tests also reveal surprisingly different properties of the MDI maps from conventional scalar maps which we attribute to the complex relation between the orientation of the field and the polarization signal. We conclude that the information about the field is primarily extracted from the changes in magnetic orientation due to rotation rather than from the Doppler shifts critical for scalar Doppler Imaging maps making it possible to apply the MDI to even very slow rotators.

Key words. stars: magnetic fields – stars: chemically peculiar – methods: Doppler Imaging

1. Introduction

Doppler Imaging (DI) is a complex technique that is used to reconstruct features on the surfaces of stars by inverting a time-series of high-resolution spectral line profiles into a map of the stellar surface. The basic concepts of DI have been reviewed in a number of papers, which described application of this technique to the imaging of specific local parameters of the stellar photospheres. This includes temperature mapping of late-type active stars (Vogt et al. 1987; Rice & Strassmeier 2000), reconstruction of the abundance distribution on the surfaces of chemically peculiar stars (Rice et al. 1989) and imaging of the magnetic field on active late-type stars (Brown et al. 1991).

Recently Piskunov & Kochukhov (2002, hereafter Paper I) extended DI principles to the recovery of the vector magnetic fields from the rotational modulation of all four Stokes parameter datasets. Our magnetic Doppler Imaging code `INVERS10` incorporates the latest developments in polarized radiative transfer, optimization and parallel computing. It is the first DI code that is aimed at the simultaneous and self-consistent recovery of the stellar magnetic field *vector* map and a distribution of one additional scalar parameter, such as the chemical abundance for magnetic chemically peculiar stars in the current version of our code or temperature for active late-type stars in future applications of our MDI method.

Similar to all other applications of Doppler Imaging techniques, an MDI code requires extensive testing and evaluation of its performance under realistic conditions. This can be done with the help of numerical experiments. In such tests the code is used in the forward mode for calculation of the Stokes parameters for a given magnetic and abundance distribution. Synthetic Stokes spectra are convolved with the instrumental profile and a random noise component is added to simulate imperfections of real observational data. Then synthetic Stokes vectors are used by the MDI code to recover magnetic and abundance maps, which are finally compared with the initial distributions. In this paper we describe numerical tests and simulations for the domain of the early-type magnetic stars, namely for the objects with inhomogeneous surface distributions of chemical elements and well-ordered, predominantly quasidipolar magnetic fields. In future we plan to extend our work to late-type active stars, which have less organized weak fields and inhomogeneous surface temperature distributions.

2. Setup for numerical experiments

For all numerical tests we used an ATLAS9 (Kurucz 1993) model atmosphere with $T_{\rm eff} = 9000$ K and $\log g = 4.0$.

Send offprint requests to: O. Kochukhov,
e-mail: `oleg@astro.uu.se`

These stellar parameters are representative for a magnetic A-type star. We have chosen the rotational velocity $v \sin i = 30\,\mathrm{km\,s^{-1}}$ and inclination angle $i = 60°$, which are optimal for DI. In addition, modelling linear polarization profiles requires specifying the angle Θ ($0° \leq \Theta \leq 360°$) between the stellar rotational axis and the local meridian projected on the sky. We used $\Theta = 90°$ throughout this paper. Both macroturbulent and microturbulent velocities were assumed to be zero in all calculations. For the evaluation of the disk-integrated Stokes parameters we employed a spatial grid divided into 695 surface zones. This grid size proved to be adequate for the calculation of the Stokes flux profiles for the adopted value of $v \sin i$ (see Sect. 2.5.1 of Paper I for more details).

In out tests we considered magnetic geometries consisting of different combinations of a centred dipolar and a linear quadrupolar field. Each of the magnetic components can be characterized by the field strengths B_d and B_q at the corresponding magnetic poles plus unit vectors $\boldsymbol{u}_\mathrm{d} \equiv (1, \beta_\mathrm{d}, \gamma_\mathrm{d})$ and $\boldsymbol{u}_\mathrm{q} \equiv (1, \beta_\mathrm{q}, \gamma_\mathrm{q})$, specifying orientation of the dipole and quadrupole axes ($0° \leq \beta_\mathrm{d}, \beta_\mathrm{q} \leq 180°$ and $0° \leq \gamma_\mathrm{d}, \gamma_\mathrm{q} \leq 360°$). The magnetic field vector at a given point $\boldsymbol{r} \equiv (R_\star, \rho, \eta)$ on the stellar surface is given, respectively, by

$$\boldsymbol{B}_\mathrm{d}(\boldsymbol{r}) = -\frac{B_\mathrm{d}}{2}\left[\boldsymbol{u}_\mathrm{d} - 3\frac{(\boldsymbol{u}_\mathrm{d}\cdot\boldsymbol{r})}{R_\star^2}\boldsymbol{r}\right] \quad (1)$$

and

$$\boldsymbol{B}_\mathrm{q}(\boldsymbol{r}) = -\frac{B_\mathrm{q}}{2}\left[2\frac{(\boldsymbol{u}_\mathrm{q}\cdot\boldsymbol{r})}{R_\star}\boldsymbol{u}_\mathrm{q} + \frac{\boldsymbol{r}}{R_\star} - 5\frac{(\boldsymbol{u}_\mathrm{q}\cdot\boldsymbol{r})^2}{R_\star^3}\boldsymbol{r}\right]. \quad (2)$$

Here $R_\star$ denotes the stellar radius, ρ and η are the latitude ($-90° \leq \rho \leq 90°$) and the longitude ($0° \leq \eta \leq 360°$) on the stellar surface. The angles β_d and β_q are measured from the positive rotational pole (by definition the star rotates counterclockwise), while the angles γ_d and γ_q are measured in the direction of stellar rotation from the half-plane containing the rotational axis and zero stellar longitude. A definition of the stellar longitude and latitude has been detailed in Paper I. The reference magnetic topology of our DI tests consisted of a dipole with polar strength $B_\mathrm{d} = 8$ kG, positioned in the plane of the stellar rotational equator, and with the positive magnetic pole crossing the plane containing the line-of-sight and the stellar rotational axis at zero phase: $\beta_\mathrm{d} = 90°, \gamma_\mathrm{d} = 0°$. Such a magnetic geometry, rotational velocity and inclination collaborate to maximize the magnetic variability of the spectral line profiles and represent an ideal combination for the application of MDI.

All Stokes profiles in this paper were calculated for the iron doublet Fe II 6147.74 Å and 6149.26 Å. Table 1 lists atomic parameters of these transitions relevant for the magnetic spectrum synthesis. These data were extracted from the VALD atomic database (Kupka et al. 1999). The Zeeman splitting pattern was calculated with the help of expressions given in Sobelman (1979). The Fe II 6147.74 Å and 6149.26 Å spectral lines are known to have different magnetic sensitivities and serve as a primary spectral diagnostic for the surface field modulus of slowly rotating Ap stars (Mathys et al. 1997). Note, that in very strong magnetic fields ($\gtrsim$10 kG) relative positions and strengths of the π and σ components of this Fe II doublet deviate from the simple Zeeman splitting pattern. Mathys (1990) showed that in strong fields the partial Paschen-Back effect plays an important role in the formation of these spectral lines, and therefore must be taken into account in any realistic synthetic spectra calculations. However, since we are mainly interested in the numerical tests of an MDI reconstruction, not in confronting our synthetic Stokes profiles with real observations, departures from the Zeeman effect were not taken into account in our calculations.

Table 1. Atomic parameters of the Fe II doublet used in MDI calculations. Subscripts u and l correspond to the upper and lower atomic levels.

λ (Å)	$\log gf$	E_l ($\mathrm{cm^{-1}}$)	g_l	J_l	g_u	J_u
6147.741	−2.721	31 364.440	1.2	1.5	2.7	0.5
6149.258	−2.680	31 368.450	0.0	0.5	2.7	0.5

The Fe II 6149.26 Å has an unusual splitting pattern of a pure Zeeman doublet. In the regime of the Zeeman effect wavelength positions of the π and σ magnetic components coincide, resulting in Stokes Q and U to be exactly zero regardless of the field strength or orientation. Thus, in the MDI tests with four Stokes parameters we effectively used only the linear polarization signal from the Fe II 6147.74 Å line.

The abundance distribution adopted in the MDI simulations consisted either of three spots of enhanced Fe abundance located at different latitudes or a larger single spot centred on the negative magnetic pole. We used an iron abundance $\varepsilon(\mathrm{Fe}) \equiv \log(N_\mathrm{Fe}/N_\mathrm{total}) = -4.0$ outside spots and $\varepsilon(\mathrm{Fe}) = -2.5$ inside iron concentrations. For the calculations with an homogeneous Fe distribution $\varepsilon(\mathrm{Fe}) = -3.65$ was adopted for the whole stellar surface. Synthetic observational data were simulated for 10 equidistant rotational phases and convolved with the Gaussian instrumental profile with $FWHM = 61$ mÅ (corresponding to the spectral resolution $R = 100\,000$ at $\lambda = 6148$ Å). Random noise with an amplitude of $\sigma_I = 3.3 \times 10^{-3}$ ($S/N = 300$) was added to Stokes I profiles, while noise levels in Stokes V and Stokes QU were scaled down by a factor of 1.5 and 4, respectively. These values were selected in order to keep amplitudes of the circular and linear polarization signatures in the Fe II lines at the level of 3–4σ. Specific noise levels were adopted only for the modelling of the particular Fe II doublet and do not set general requirements for the spectropolarimetric data in other wavelength regions. In the case of magnetic topologies studied with `INVERS10` other stronger spectral lines (e.g. Fe II 4923.93 Å and Fe II 5018.44 Å) show linear and circular polarization signatures with much higher amplitudes and can be detected at the 3σ level with a S/N of 150–200 in Stokes Q and

Table 2. Numerical tests of the MDI code. Parameters of the global magnetic distributions are given for a dipolar field D in the form $(B_{\rm d}, \beta_{\rm d}, \gamma_{\rm d})$, for an axisymmetric quadrupole Q as $(B_{\rm q}, \beta_{\rm q}, \gamma_{\rm q})$ and for magnetic spots of test No. 3 as (field strength in the spot $B_{\rm spot}$, spot latitude $\rho_{\rm spot}$ and spot longitude $\eta_{\rm spot}$). The field strengths $B_{\rm d}$, $B_{\rm q}$ and $B_{\rm spot}$ are given in kG. The stellar parameters are represented as $v \sin i$ in $\mathrm{km\,s^{-1}}$ and angles i and Θ in degrees. $\delta\varepsilon$, δB, $\delta\rho$ and $\delta\eta$ are the average errors of the recovery of abundance, magnetic field strength, and meridional and azimuthal orientations of the magnetic field vectors.

Test No.	Surface distributions ε(Fe)	magnetic field model	Stellar parameters	Obs. data	Recovery of	$\delta\varepsilon$ (%)	δB (%)	$\delta\rho$ (°)	$\delta\eta$ (°)
1		*Reference test model*							
	no spots	D:(8, 90°, 0°)	30, 60°, 90°	$IQUV$	$\varepsilon, \boldsymbol{B}$	6.3	6.8	4.6	2.4
	1 spot	D:(8, 90°, 0°)	30, 60°, 90°	$IQUV$	$\varepsilon, \boldsymbol{B}$	7.6	8.7	4.7	3.1
2		*Complex global magnetic distributions*							
	no spots	Q:(8, 90°, 0°)	30, 60°, 90°	$IQUV$	$\varepsilon, \boldsymbol{B}$	9.8	9.3	10.3	5.0
	no spots	D:(8, 90°, 0°)+Q:(8, 90°, 0°)	30, 60°, 90°	$IQUV$	$\varepsilon, \boldsymbol{B}$	7.1	7.5	4.4	2.7
	no spots	D:(8, 90°, 0°)+Q:(8, 90°, 90°)	30, 60°, 90°	$IQUV$	$\varepsilon, \boldsymbol{B}$	6.8	5.6	4.0	2.5
	3 spots	Q:(8, 90°, 0°)	30, 60°, 90°	$IQUV$	$\varepsilon, \boldsymbol{B}$	14.1	16.0	15.3	11.1
	3 spots	D:(8, 90°, 0°)+Q:(8, 90°, 0°)	30, 60°, 90°	$IQUV$	$\varepsilon, \boldsymbol{B}$	15.5	11.1	8.3	5.7
	3 spots	D:(8, 90°, 0°)+Q:(8, 90°, 90°)	30, 60°, 90°	$IQUV$	$\varepsilon, \boldsymbol{B}$	13.7	15.9	9.9	6.6
3		*Non-global magnetic distribution*							
	no spots	two spots (8, 0°, 0°)+(−8, 0°, 180°)	30, 60°, 90°	$IQUV$	$\boldsymbol{B}$	—	21.3	3.4	1.1
	no spots	two spots (8, 0°, 0°)+(−8, 0°, 180°)	30, 60°, 90°	IV	$\boldsymbol{B}$	—	45.8	20.4	3.1
4		*MDI of slow rotators*							
	3 spots	D:(8, 90°, 0°)	30, 60°, 90°	$IQUV$	$\varepsilon, \boldsymbol{B}$	11.1	10.5	6.5	3.5
	3 spots	D:(8, 90°, 0°)	10, 60°, 90°	$IQUV$	$\varepsilon, \boldsymbol{B}$	13.8	5.4	5.1	2.6
	3 spots	D:(8, 90°, 0°)	5, 60°, 90°	$IQUV$	$\varepsilon, \boldsymbol{B}$	13.3	4.5	4.4	2.8
	3 spots	no magnetic field	5, 60°, 90°	I	ε	88.7	—	—	—
5		*Non-optimal orientations of the stellar and magnetic axes*							
	no spots	D:(8, 90°, 0°)	30, 30°, 90°	$IQUV$	$\varepsilon, \boldsymbol{B}$	5.5	6.0	3.4	1.8
	no spots	D:(8, 30°, 0°)	30, 60°, 90°	$IQUV$	$\varepsilon, \boldsymbol{B}$	7.4	5.2	6.3	4.4
	no spots	D:(8, 60°, 0°)	30, 60°, 90°	$IQUV$	$\varepsilon, \boldsymbol{B}$	6.1	5.3	3.7	2.1
	no spots	D:(8, 45°, 0°)	30, 90°, 90°	$IQUV$	$\varepsilon, \boldsymbol{B}$	9.1	4.3	4.7	2.4
6		*Errors in the input parameters*							
	no spots	D:(8, 90°, 0°)	27, 60°, 90°	$IQUV$	$\boldsymbol{B}$	—	20.0	15.1	6.9
	no spots	D:(8, 90°, 0°)	33, 60°, 90°	$IQUV$	$\boldsymbol{B}$	—	19.2	38.1	17.3
	no spots	D:(8, 90°, 0°)	30, 40°, 90°	$IQUV$	$\boldsymbol{B}$	—	9.4	7.9	2.9
	no spots	D:(8, 90°, 0°)	30, 80°, 90°	$IQUV$	$\boldsymbol{B}$	—	7.0	10.1	3.0
	no spots	D:(8, 90°, 0°)	30, 60°, 120°	$IQUV$	$\boldsymbol{B}$	—	15.0	28.2	14.4
7		*Reduced quality of the observational data*							
	3 spots	D:(8, 90°, 0°)	5 phases	30, 60°, 90°	$IQUV$	$\varepsilon, \boldsymbol{B}$	18.6	17.7	11.5	6.1
	3 spots	D:(8, 90°, 0°)	phase gap of 0.3	30, 60°, 90°	$IQUV$	$\varepsilon, \boldsymbol{B}$	18.3	14.9	11.1	3.8
	3 spots	D:(8, 90°, 0°)	$R = 20\,000$	30, 60°, 90°	$IQUV$	$\varepsilon, \boldsymbol{B}$	22.0	12.4	8.0	3.5
	3 spots	D:(8, 90°, 0°)	$\sigma_I = 1.7 \times 10^{-2}$	30, 60°, 90°	$IQUV$	$\varepsilon, \boldsymbol{B}$	42.3	22.6	14.2	7.8

U and a S/N of 30–50 in Stokes V. As for real applications of the MDI, medium strength or moderately strong spectral lines with a high amplitude of linear polarization signatures are the best. For cool Ap stars such spectral features can be selected using an atlas of Zeeman polarization in the spectrum of β CrB published by Wade et al. (2000b).

In all test inversions with four Stokes parameters we used the Tikhonov regularization functional to regularize reconstructed maps of the abundance and magnetic field vector. Our detailed investigation of the role of regularization in the MDI (see Sect. 2.7 of Paper I) showed that this type of regularization function ensures the smooth convergence to the optimal maps but does not impose any global constraints on the final magnetic geometry. The regularization parameter was selected in such a way that at convergence the regularization functional and χ^2 of the fit to simulated observations gave approximately equal contributions to the total discrepancy function. In the MDI experiments based on circular polarization data alone (Sect. 10) the multipolar regularization function introduced in Paper I was used together with the Tikhonov functional in order to improve recovery of the magnetic field. At the same time abundance images were still regularized by the Tikhonov functional alone.

We note that in our four Stokes parameter Doppler Imaging based on the inversion technique with the Tikhonov regularization no global constraints are imposed on the large scale field structure and therefore the resulting magnetic distribution does not necessarily satisfy Maxwell's equations. This problem is common for all applications of unconstrained Doppler reconstruction of the

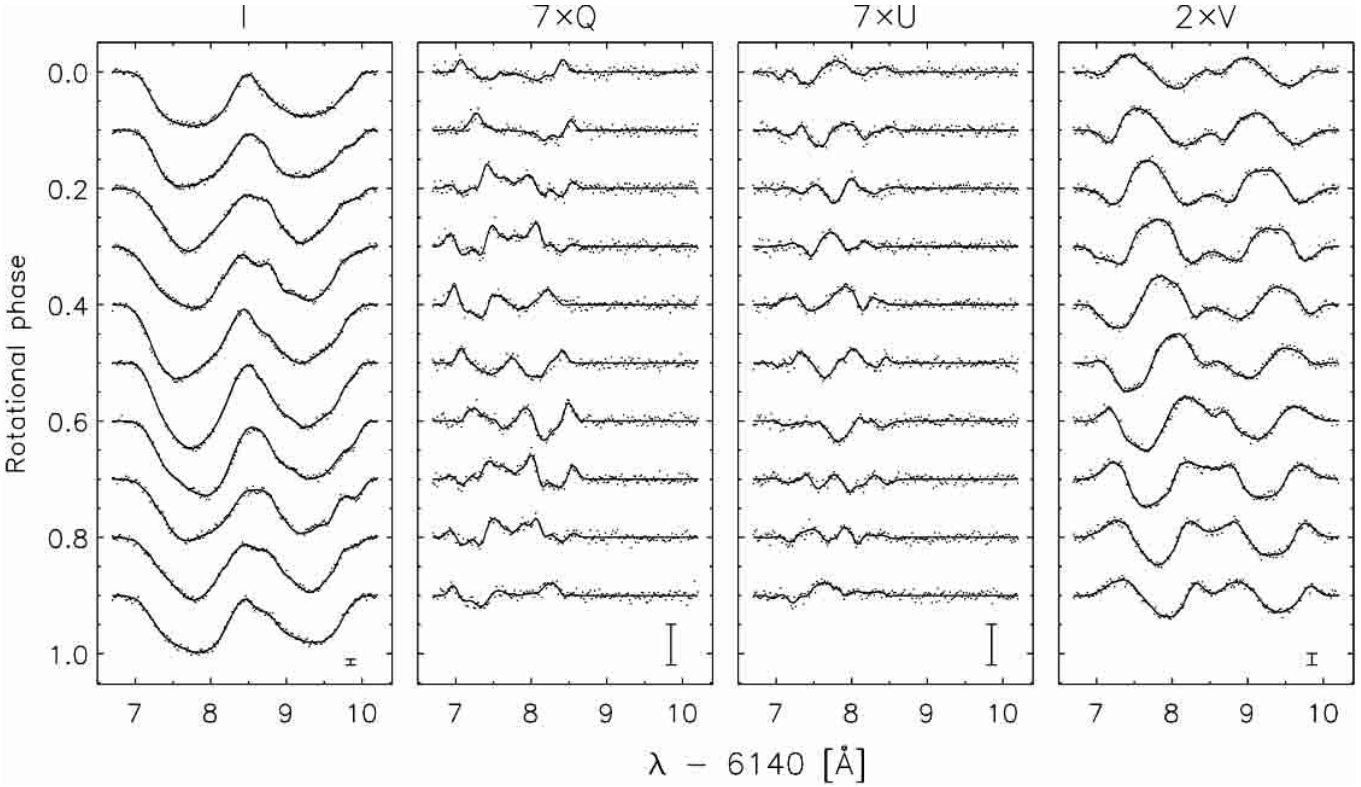

Fig. 1. Synthetic Stokes I, Q, U and V profiles of the Fe II 6147.74 and 6149.26 Å spectral lines for the reference test distribution (Fig. 3). Simulated observational data is shown by dots, while solid lines represent the final fit by the MDI code. Profiles for consecutive rotational phases are shifted in the vertical direction. Note, the different scale used for Stokes I profiles, circular and linear polarization. The bar at the lower right of each Stokes parameter plot corresponds to 1% of the continuum level of Stokes I.

stellar magnetic fields (e.g. Donati 2001). However, in reality due to the incomplete phase coverage, visibility and projection effects or/and additional abundance or temperature inhomogeneities there always exist areas on the stellar surface for which even the best spectropolarimetric dataset cannot provide reliable information about the surface structures. Therefore, we believe that in all real applications it is possible to find solutions within the uncertainty of the final magnetic map that would obey integral constraints imposed by Maxwell's equations.

Since the parameter space of the possible MDI experiments is enormous, we decided to explore the space around the model that was detailed above (we call it the *reference model*), not departing very far from it. In this sense testing of our MDI code was necessarily restricted. Table 2 summarises basic types of conducted numerical experiments. In the second and third column, after the test number, we give brief description of the surface abundance and magnetic geometries. The next column contains the information about the stellar parameters that were used in the recovery of the surface maps. The fifth column specifies observational data used in MDI tests, while the sixth lists a variable recovered in the DI inversion (iron abundance ε(Fe) or/and vector magnetic field $\boldsymbol{B}$). The rest of the table contains numerical assessment of the average reconstruction errors of the abundance $\delta\varepsilon$, magnetic field modulus δB, azimuthal $\delta\eta$ and meridional $\delta\rho$ orientation of the magnetic vectors. These quantities were calculated using the following expression:

$$\delta M = \sqrt{\sum_j \omega_j^2 \left(1 - \frac{M'_j}{M_j}\right)^2 / \sum_j \omega_j^2}, \tag{3}$$

where M is either abundance $10^{\varepsilon(\mathrm{Fe})}$ or field modulus B surface distributions, index j runs over all surface zones and primed variables correspond to the reconstructed maps, while unprimed denote the true distributions. In order to prohibit strong influence of the errors in low-latitude zones on the error estimates δM we used a weight function ω:

$$\omega = \begin{cases} \sin(\rho + i), & \text{for } \rho \geq -i \\ 0, & \text{for } \rho < -i \end{cases}, \tag{4}$$

where ρ is the latitude on the stellar surface and i denotes inclination angle of the stellar rotational axis. In Paper I we found that a simple sine law adopted for ω gives reasonable approximation of the average latitude dependence of the discrepancy between the true and recovered maps. Average errors of the reconstructed field orientation (measured in degrees) were estimated as

$$\delta\xi = \sqrt{\sum_j (\omega'_j \, \Delta\xi_j)^2 / \sum_j (\omega'_j)^2}, \tag{5}$$

where $\Delta\xi$ is either meridional $\Delta\rho$ or azimuthal $\Delta\eta$ angles between the true and recovered directions of the local magnetic vectors. The weight function ω' gives a larger weight to the areas with larger field strength: $\omega' = B\omega$.

Besides calculation of the average local errors of the MDI reconstruction, we also tested how well global magnetic structures were resolved by `INVERS10`. For this purpose the final magnetic maps were expanded into real spherical harmonics up to second order using a weighted least-squares scheme described in Appendix A of Paper I. From the set of expansion coefficients dipole and quadrupole parameters were determined and compared with their true values. Our parameterization of the global magnetic field is identical to the one used by Landolfi et al. (1998), except that we measure the azimuth angles γ of the dipole and quadrupole axes from the same half-plane as described above.

In addition to the numerical assessment of the MDI reconstruction quality, Figs. 2–13 show graphical comparisons between the true and recovered maps. In the next Sections we give detailed description of the most important numerical simulations.

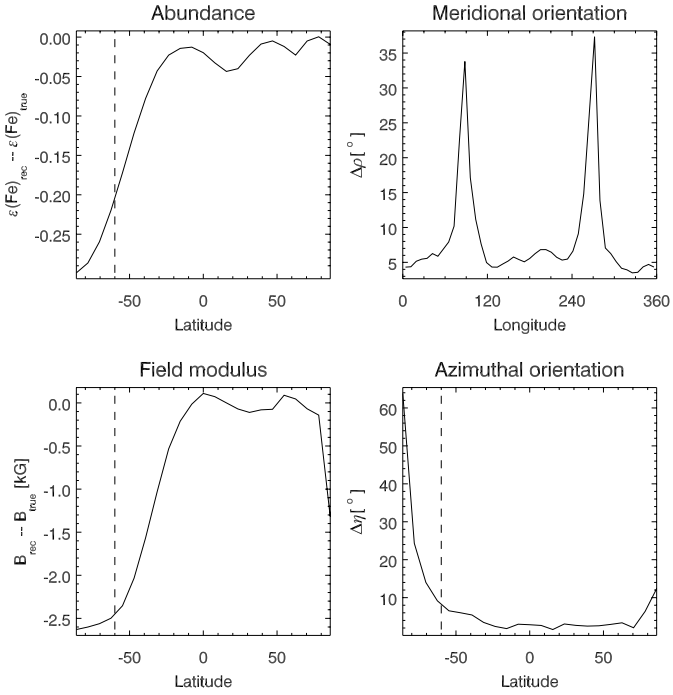

Fig. 2. The average latitude dependence of the difference between the true and recovered abundance, field strength and the azimuthal angle between the true and reconstructed field vectors. For the corresponding meridional angle the average longitude trend is displayed. In all latitude plots the vertical dashed line shows the lowest visible latitude for the adopted inclination angle $i = 60°$. This figure refers to the reconstruction of the reference magnetic topology and homogeneous abundance distribution.

3. Reconstruction of the reference test distribution

In the first MDI test `INVERS10` reconstructed a dipolar magnetic distribution using the full Stokes vector observational dataset. The abundance map consisted of a single Fe spot, located on the negative magnetic pole. The initial guess for this MDI inversion was zero magnetic field and an homogeneous iron distribution with $\varepsilon(\mathrm{Fe}) = -4.0$. All stellar parameters were assumed to be known exactly. Figure 1 shows the comparison between simulated Stokes I, Q, U and V observational data and the final fit achieved by `INVERS10`. The comparison between the true and recovered abundance and magnetic maps is displayed in Fig. 3. In this and other similar plots the star is shown at 5 equidistant rotational phases and an inclination angle, corresponding to the value adopted for MDI recovery ($i = 60°$ in this and most other tests). The black and grey arrows show areas of the positive and negative magnetic field respectively; orientations of the arrows correspond to the orientations of the local magnetic field vectors, while the lengths of the arrows are proportional to the field strength. Magnetic maps are displayed on the same surface grid that was used for the disk integration and inversion. Greyscale images underlying vector magnetic maps show the distribution of the field modulus, while Fe concentrations are highlighted on the separate abundance maps.

Figure 3 confirms that in general the quality of the simultaneous recovery of the three magnetic vector components and iron distribution is very good. The latitudinal and longitudinal position of the abundance spot was recovered with high accuracy, similar to the results of non-magnetic DI tests (e.g. Piskunov & Wehlau 1990). High-contrast edges of the Fe spot were somewhat smeared out in the reconstructed image, but this is to be expected with the modest sampling of the rotational period and with the Tikhonov regularization that we used. The magnetic map was properly recovered over the whole stellar surface with the exception of a few low-latitude belts, which have negligible impact on the disk-integrated Stokes signal and therefore retained a weaker magnetic field, closer to the zero-field initial guess. The average error of the abundance recovery was 8% (which corresponds to only 0.04 in $\log(N_{\mathrm{Fe}}/N_{\mathrm{total}})$ units), while the field modulus was reconstructed on average within 9% of the true map. The meridional and azimuthal directions of the local magnetic vectors were restored within 5°, with the azimuthal orientation recovered better than meridional.

`INVERS10` is the first MDI code that attempts simultaneous recovery of non-parameterized magnetic and abundance maps. Therefore the method is potentially prone to systematic errors due to the crosstalk between magnetic and abundance maps. We investigated this problem by carrying out the same magnetic DI inversion, but using a homogeneous Fe distribution. The initial guess for the Fe abundance was also an homogeneous map, but with an incorrect $\varepsilon(\mathrm{Fe})$ value. `INVERS10` was again allowed to vary both the magnetic and abundance distributions. As a result, the magnetic dipolar field was recovered with the same quality as in the test with the abundance spot. No global structures tracing the magnetic dipole pattern

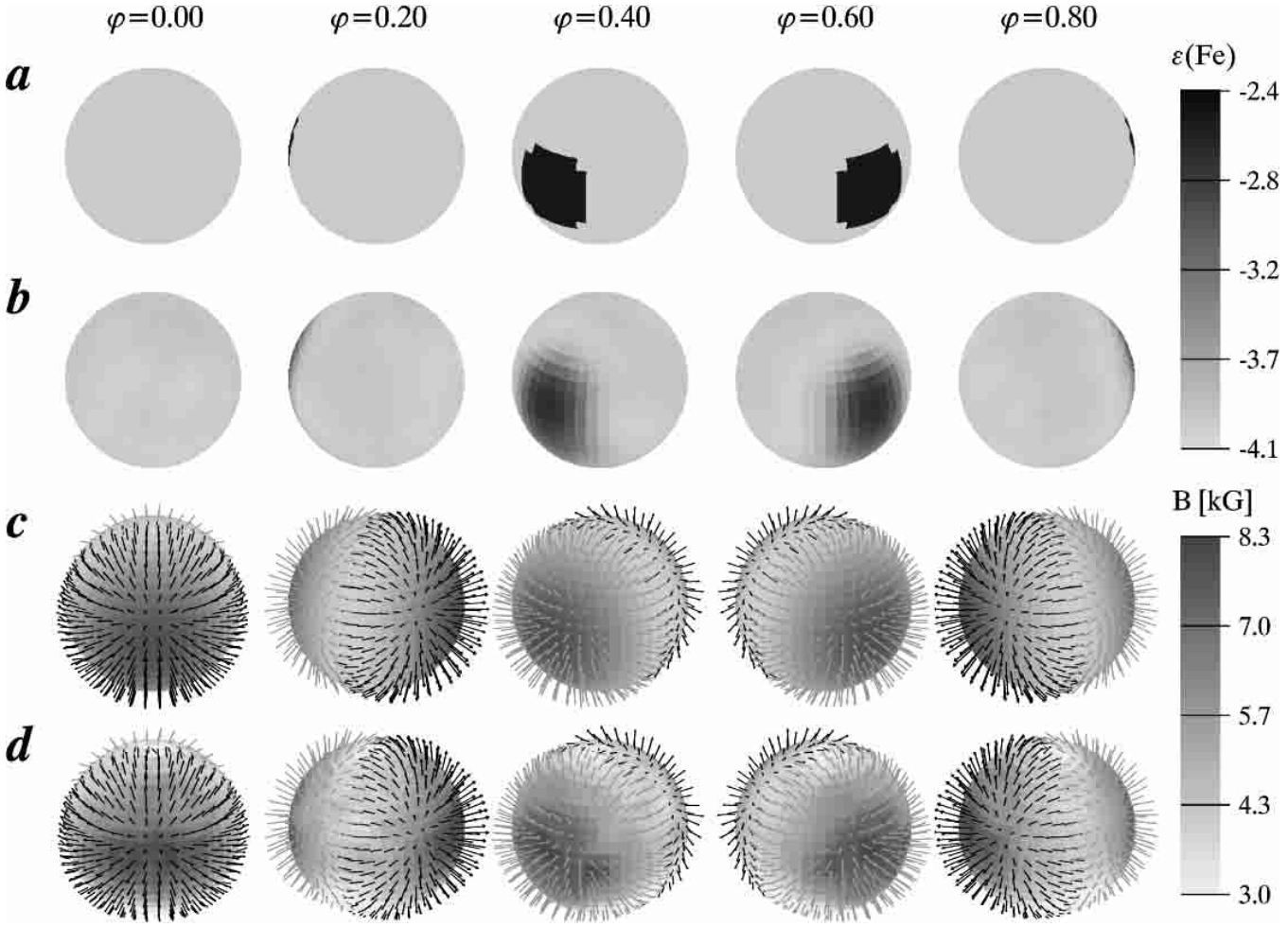

Fig. 3. Simultaneous recovery of the Fe abundance distribution and dipolar magnetic field using Stokes vector data of Fig. 1. The true abundance **a)** and magnetic **c)** maps are compared with the restored Fe abundance **b)** and magnetic **d)** images. The black arrows show field vectors pointing outside the stellar surface, while grey arrows correspond to the vectors pointing inwards. The arrow length is proportional to the field strength. Greyscales of the images **a)** and **b)** correspond to the iron abundance, while greyscales of the images **c)** and **d)** visualize the distribution of the magnetic field modulus. The star is shown at 5 equidistant rotational phases, viewed at the inclination angle $i = 60^\circ$ with the rotational axis oriented in the vertical direction.

were found in the recovered Fe distribution, which deviated from the true abundance map by less than 10% on average. Thus, our MDI reconstruction is free from crosstalk between magnetic and abundance images.

For the last experiment the analysis of the average coordinate dependencies of the errors in recovered maps gives additional information about `INVERS10` performance. Basically abundance, field strength and azimuthal direction errors contain only latitude dependence. Figure 2 shows that the quality of the field modulus recovery is acceptable from the rotational pole down to 20–25° below the rotational equator, i.e. within 50–55° from the line-of-sight. Closer to the invisible rotational pole field strength is underestimated by as much as 1–2 kG. The quality of the abundance and azimuthal direction recovery is homogeneously good from the rotational pole to subequatorial regions. These errors increase only for the lowest latitude belts, which are strongly influenced by the initial guess. In contrast, the meridional angle between the true and recovered field vectors shows mostly longitudinal dependence. The error is the largest in areas close to the intersection between the rotational and magnetic equators, i.e. where the meridional component of the adopted magnetic distribution is very weak. We found that these average trends of the quality of the abundance and magnetic field recovery are typical for all MDI tests with `INVERS10`.

Another important issue in Doppler Imaging reconstruction is the dependence of magnetic DI images on the adopted initial guess. This problem was studied by conducting two more inversions, which were similar to the reference test with the homogeneous Fe distribution with the exception, that different non-zero initial guesses were used for the field distribution. In one experiment MDI inversion started from an homogeneous radial field with $B_\mathrm{r} = 5$ kG, while in the other test the true dipolar distribution was rotated by 90° in the longitudinal direction (γ_d was 90° instead of 0°) and adopted as the initial guess. Although the initial distributions were altered considerably, the average `INVERS10` reconstruction errors were found to be approximately the same as with the zero-field initial guess.

The recovered vector distributions were not different either: only the lowest visible latitude belts retained some imprint of the initial guess.

The quality of the recovery of global magnetic structures was tested by expanding recovered maps into spherical harmonics up to the second order. This is equivalent to finding the best-fit parameters of a combination of a magnetic dipole and a non-axisymmetric quadrupole. We found that for all magnetic maps reconstructed in test No. 1, polar strength of the dipole was underestimated by 0.3–0.5 kG (5–6% of $B_{\rm d}$), while the contribution of the quadrupolar component (absent in the true magnetic geometry) was below 0.7 kG. The orientation of the dipole was recovered within 1° in latitude and 0.5° in longitude.

In general, numerical results of the simultaneous recovery of the abundance distribution and dipolar magnetic geometry build up firm evidence that *the MDI technique provides an accurate, self-consistent reconstruction of the abundance and magnetic maps without any a priori assumptions about global stellar magnetic topology.*

4. Reconstruction of complex global magnetic geometries

Although the global magnetic fields of chemically peculiar stars are traditionally considered to be predominantly dipolar, recent investigations (e.g. Bagnulo et al. 1999; Landstreet & Mathys 2000) found evidence for the strong contribution of higher-order multipoles in magnetic geometry. Similar deviations from the simplest dipolar magnetic topology were also found for the magnetic white dwarfs (Wickramasinghe & Ferrario 2000). Due to the averaging over the stellar disk, quadrupole and higher multipoles produce relatively weak contributions to the most common magnetic observable, longitudinal field, and thus elude detection. Only a simultaneous fit to many magnetic observables or direct analysis of the information contained in the line profiles of the Stokes parameters helps to reveal true magnetic geometry. Since a pure dipolar field is found for only a minor fraction of stars, studied with modern methods, it is reasonable to speculate that the majority of magnetic CP stars and white dwarfs possess non-dipolar fields. Therefore it is important to study the performance of the MDI code in the recovery of such complex global magnetic distributions.

In test No. 2 `INVERS10` recovered two combinations of a dipolar and axisymmetric quadrupolar fields with $B_{\rm d} = B_{\rm q} = 8$ kG. For the first experiment we adopted a configuration in which the dipole and quadrupole were aligned ($\beta_{\rm d} = \beta_{\rm q} = 90°, \gamma_{\rm d} = \gamma_{\rm q} = 0°$; Fig. 4a), effectively doubling the field strength on the positive pole and reducing the negative polar strength to zero. In the other experiment the quadrupole axis was assumed to lie in the same (equatorial) plane as the dipole axis ($\beta_{\rm d} = \beta_{\rm q} = 90°$), but rotated in the longitudinal direction by 90° with respect to the dipole axis ($\gamma_{\rm d} = 0°, \gamma_{\rm q} = 90°$; Fig. 4c). Such a magnetic combination produces a complex, non-axisymmetric magnetic map, which is characterized by a sector of the strong negative field covering only a quarter of the stellar surface, while the rest is occupied by a weaker positive field. In addition to the tests with two different combinations of the dipolar and quadrupolar fields we also attempted reconstruction of a purely quadrupolar magnetic topology ($B_{\rm q} = 8$ kG, $\beta_{\rm q} = 90°, \gamma_{\rm q} = 0°$; Fig. 4e). Two series of tests have been carried out with all three magnetic configurations. First we reconstructed the magnetic field and an homogeneous abundance distribution in order to check for the crosstalk between the abundance and complex magnetic images. Then inversions were repeated for the same magnetic geometries, but now with the more complex abundance distribution, consisting of three spots of iron overabundance located at different latitudes. This second series of tests is probably the most representative of the actual surface structures on a substantial fraction of magnetic CP stars.

Three input magnetic distributions as well as the magnetic images recovered by `INVERS10` in the experiments with the complex abundance maps are presented in Fig. 4, while Fig. 5 compares the true and reconstructed surface distributions of iron. The MDI code achieved fairly good results in the magnetic reconstruction. The true and recovered maps are hardly distinguishable in Fig. 4. The only difference is the field strength in low-latitude belts, which is systematically underestimated in the reconstructed maps. The average recovery errors and their major trends are comparable to the results of test No. 1. Similarly, an homogeneous abundance distribution, recovered simultaneously with the non-dipolar magnetic field, does not reveal any crosstalk between magnetic and abundance maps. Reconstruction of the complex magnetic topologies in the presence of abundance spots resulted in magnetic images with stronger deviation from the original distributions than in the tests with an homogeneous iron abundance. However, the average errors of the recovery of the magnetic field strength and direction remain below ≈15% and inversions can be considered a success.

Multipolar expansion of the recovered magnetic images showed that for the three magnetic configurations of test No. 2 the dipole and quadrupole polar strengths were underestimated by 0.3–0.5 kG in the tests with an homogeneous abundance map and by 0.4–0.9 kG in the inversions with a spotty iron distribution. Meridional orientation of the magnetic axes was recovered typically within 7° of the true values and azimuthal orientation – within 4°.

Results of the second test series allow us to conclude, that *MDI with* `INVERS10` *is not restricted to the simplest dipolar magnetic geometries.* Furthermore, *our Doppler Imaging code is successful in the simultaneous recovery of fairly complex magnetic and abundance distributions.*

5. Recovery of a non-global magnetic distribution

Numerical simulations in our paper are concentrated mostly on global magnetic geometries, typical for magnetic CP stars. Nevertheless, in this subsection we carried out two exploratory tests of the recovery of a non-global

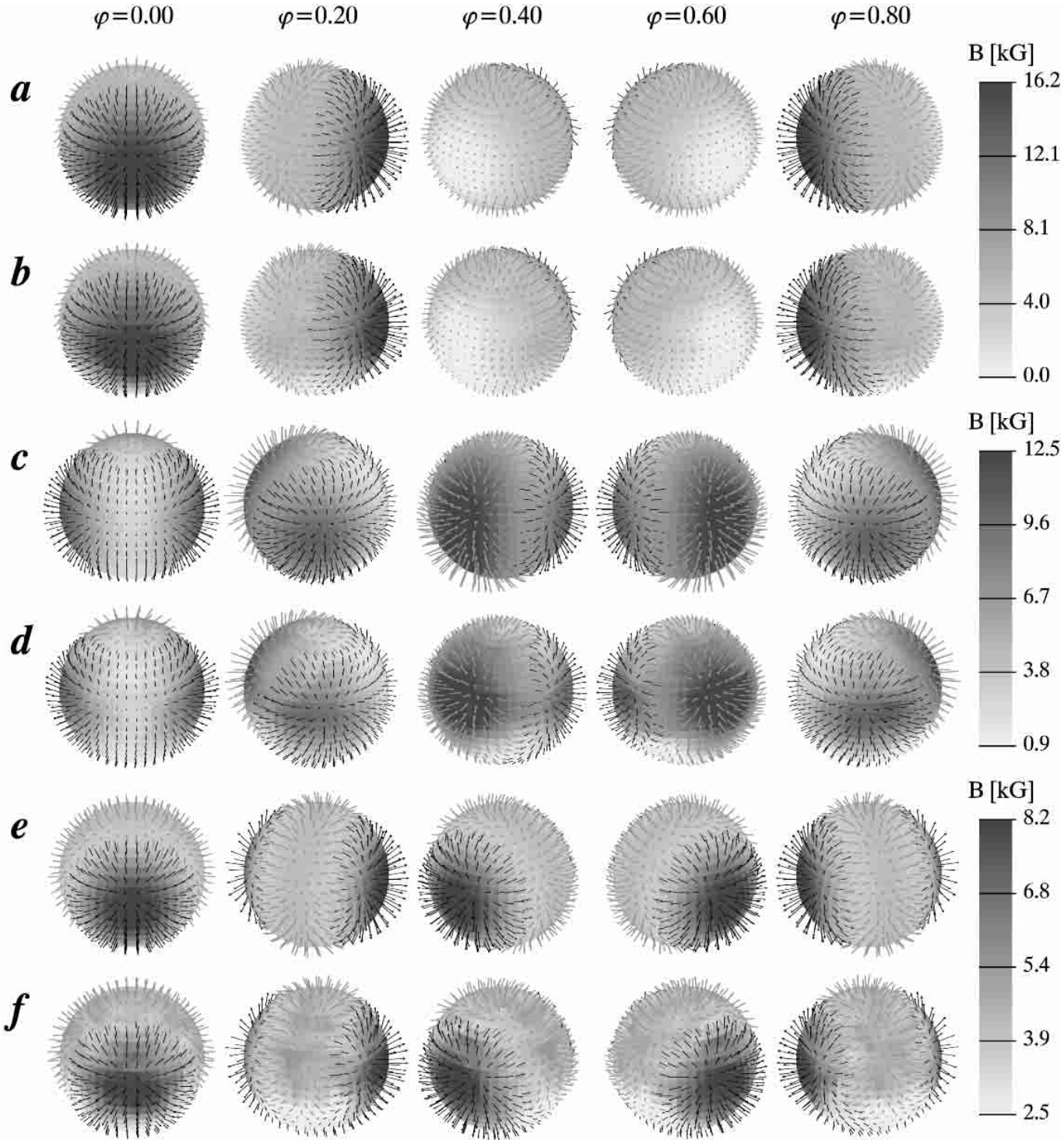

Fig. 4. Reconstruction of the complex global fields formed by the three different superpositions of a magnetic dipole and quadrupole. **a)**, **c)** and **e)** are the true maps used to simulate observations in four Stokes parameters, while **b)**, **d)** and **f)** are magnetic images recovered by the MDI code.

magnetic topology. The main goal of these experiments was to test `INVERS10`'s ability to resolve sharp magnetic structures, covering limited areas on the stellar surface, as well as to make a qualitative comparison with the results of the previous MDI simulations, conducted for the late-type magnetic stars by Brown et al. (1991) and Donati & Brown (1997). We did not aim at thorough modelling of the magnetic and temperature spots on active stars. Such a project certainly requires incorporation of an inhomogeneous temperature distribution, weaker magnetic fields and employment of the model atmospheres and spectral line list, relevant for the late-type stars. Instead, the only modification with respect to the standard setup of our numerical experiments was a magnetic field model which was

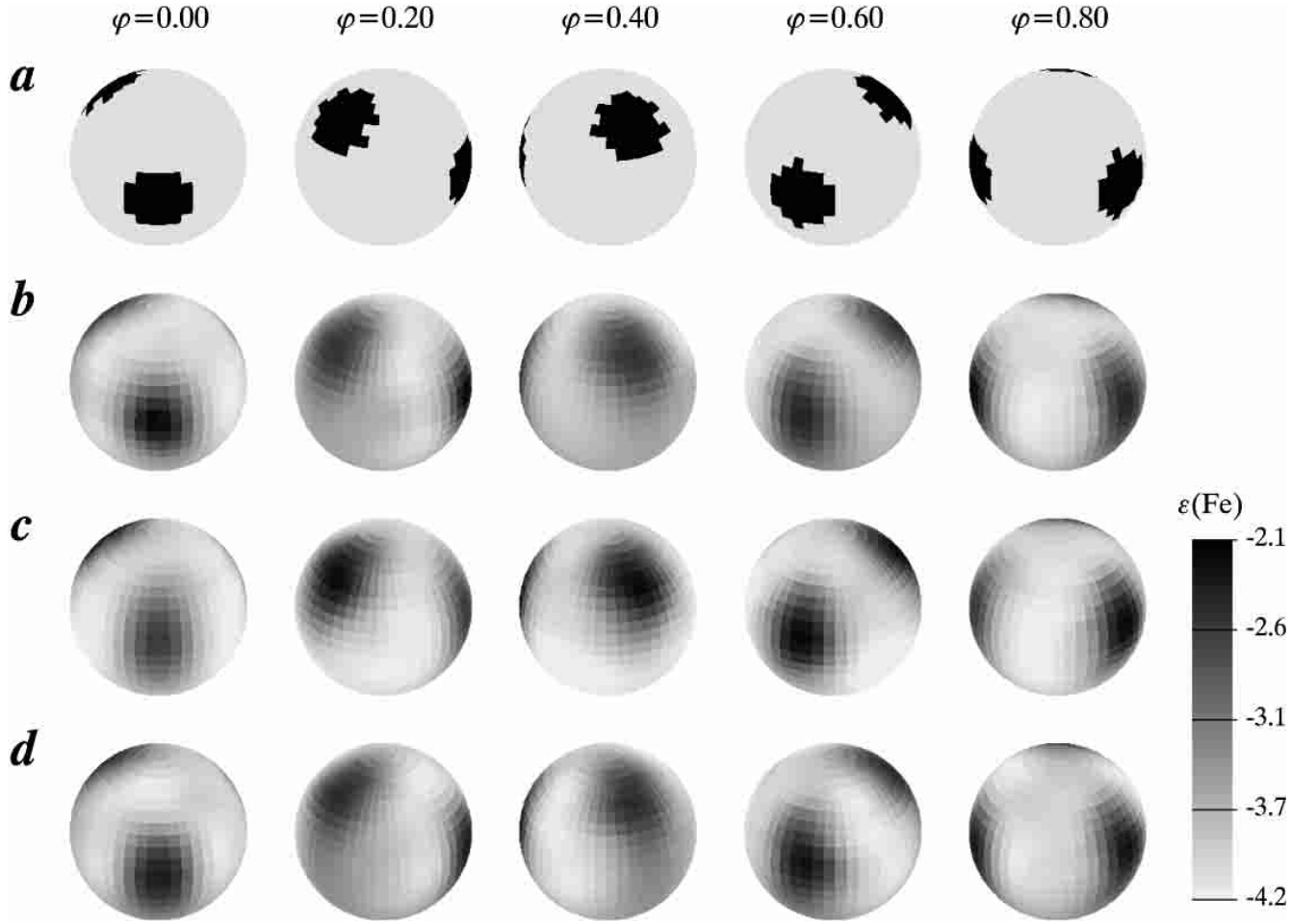

Fig. 5. Abundance distributions recovered simultaneously with the complex non-dipolar magnetic topologies. The true abundance map **a)** is compared with the abundance distributions **b–d)** reconstructed with the magnetic field maps shown in, respectively, panels **b)**, **d)** and **f)** of Fig. 4.

assumed to consist of two circular spots filled with homogeneous radial field $B_{\rm r}^{(1)} = 8$ kG and $B_{\rm r}^{(2)} = -8$ kG, having identical radii of $R_{\rm spot}^{(1)} = R_{\rm spot}^{(2)} = 0.3R_\star$. Both spots lie on the rotational equator and cross the plane containing the line-of-sight and stellar rotational axis at phases 0.0 (positive spot) and 0.5 (negative spot). Figure 6 shows this magnetic configuration and compares it with the results of the MDI recovery. In this inverse problem the iron abundance was fixed, but the magnetic distribution was imaged without any assumptions about field orientation (i.e. the full vector magnetic map was extracted from the rotational modulation of Stokes parameters).

We found that good reconstruction of the non-global magnetic topology was achieved in the experiment in which the full Stokes vector dataset was used. Positions and sizes of the magnetic spots were recovered correctly by `INVERS10`. The formal field strength error listed in Table 2 (21%) reflects smearing on the sharp edges of the magnetic spots, but apart from this problem the field modulus was recovered with an acceptable accuracy, while meridional and azimuthal orientations of the local magnetic vectors were reconstructed typically within 3° of the correct directions.

Recovered magnetic images changed substantially when observational data used for MDI were restricted to Stokes I and V parameters. Since the late-type stars possess weak fields, Stokes Q and U profiles cannot be reliably measured with existing spectropolarimeters, hence using only circular polarization profiles in the MDI of late-type active stars reflects a real deficiency of the current observational data. Figure 6 shows that reduction of the sensitivity to the transverse magnetic component leads to an underestimate of the area covered by the magnetic spots at low latitudes and, more prominently, to the strong crosstalk from the radial to meridional field map. While the average recovery error of the field modulus doubled in comparison with the MDI recovery from all four Stokes parameters, the average meridional error $\delta\rho$ increased by a factor of 10 and reached 20°. The azimuthal direction is still recovered properly, in particular no crosstalk from the radial to azimuthal maps is evident in Fig. 6.

Results of IV MDI recovery with `INVERS10` are fully consistent with similar Zeeman-Doppler imaging tests of Donati & Brown (1997), who also noticed a clear crosstalk between the radial and meridional magnetic features at low latitudes. This ambiguity of MDI images is explained

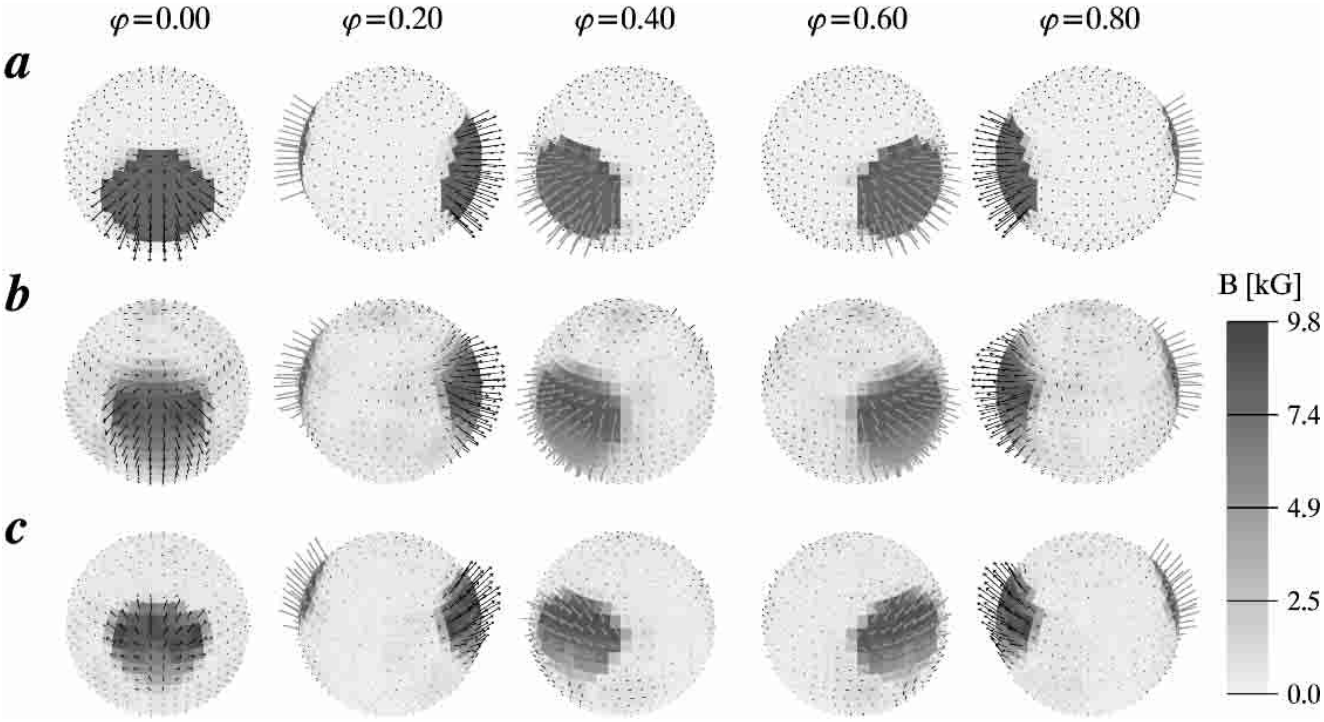

Fig. 6. Recovery of the image consisting of two magnetic spots with 8 kG radial field of the opposite polarity. The true distribution **a)** is compared with the MDI results obtained using the full Stokes vector dataset **b)** and only Stokes I and V line profiles **c)**.

by the fact that low-latitude meridional field remains transverse during most of the stellar rotational period, and therefore its influence on Stokes I and V spectra is negligible.

The two-spot experiment confirmed *the ability of* `INVERS10` *to resolve sharp non-global magnetic structures using variability of Stokes I, Q, U and V parameters.* At the same time, *sensitivity of the MDI code to the low-latitude radial magnetic fields is severely reduced for imaging with Stokes I and V only.* This leads to the ambiguity between the radial and meridional fields in the low-latitude regions.

6. MDI of slowly rotating stars

A significant fraction of chemically peculiar stars with surface fields above 1 kG have projected rotational velocities as low as 5–10 $\mathrm{km\,s^{-1}}$. Due to the sharpness of their spectral features, such stars are the best candidates for spectropolarimetric measurements in four Stokes parameters (Wade et al. 2000a). On the other hand, slowly rotating CP stars were not considered to be optimal targets for abundance DI, simply because rotational Doppler broadening does not dominate their line profiles. It is of great interest to verify the extent to which magnetic DI can use additional spectropolarimetric data and rotational modulation of the Zeeman shifts to extract useful information from the time series of four Stokes parameters, recorded for sharp line magnetic stars. In order to study this problem and to establish a lower limit of $v \sin i$ useful for MDI, we reconstructed dipolar magnetic field and Fe abundance maps for stars rotating with $v \sin i = 30$, 10 and 5 $\mathrm{km\,s^{-1}}$. The abundance distribution, adopted for these experiments, was more complex than the single-spot map of the reference test and consisted of the three areas of an enhanced iron abundance located at latitudes 0° and 60° and equidistantly spaced in longitudes.

Figures 8 and 9 show results of the simultaneous recovery of the magnetic field and Fe abundance maps for different values of $v \sin i$. Figure 7 compares synthetic observational data for the test with $v \sin i = 10$ $\mathrm{km\,s^{-1}}$ and the final fit achieved by `INVERS10`. Apparently, the quality of the magnetic and abundance imaging does not noticeably worsen with decreasing $v \sin i$. For all three test cases the average abundance and field strength errors are at the level of 10–15%, while the field direction is recovered within 3–6° of the true orientation. The global properties of the dipolar magnetic distribution were recovered even better for slowly rotating stars: a dipolar strength of $B_\mathrm{d} = 7.1$ kG was found for $v \sin i = 30$ $\mathrm{km\,s^{-1}}$ test, with a spurious $B_\mathrm{q} = 0.8$ kG quadrupolar component also present, while for the reconstructions with $v \sin i = 10$ and 5 $\mathrm{km\,s^{-1}}$ multipolar expansion of the final magnetic maps gave $B_\mathrm{d} = 7.7$ kG and $B_\mathrm{q} = 0.7$ kG. In all tests `INVERS10` reconstructed the orientation of the dipolar axis, which differed by just 1–3° from its true direction.

Additional experiments showed that magnetic Doppler Imaging provides reliable information about stellar magnetic topology down to $v \sin i = 0$ $\mathrm{km\,s^{-1}}$. However, for the extremely slow rotators the combination of instrumental and thermal Doppler broadening does not allow to resolve

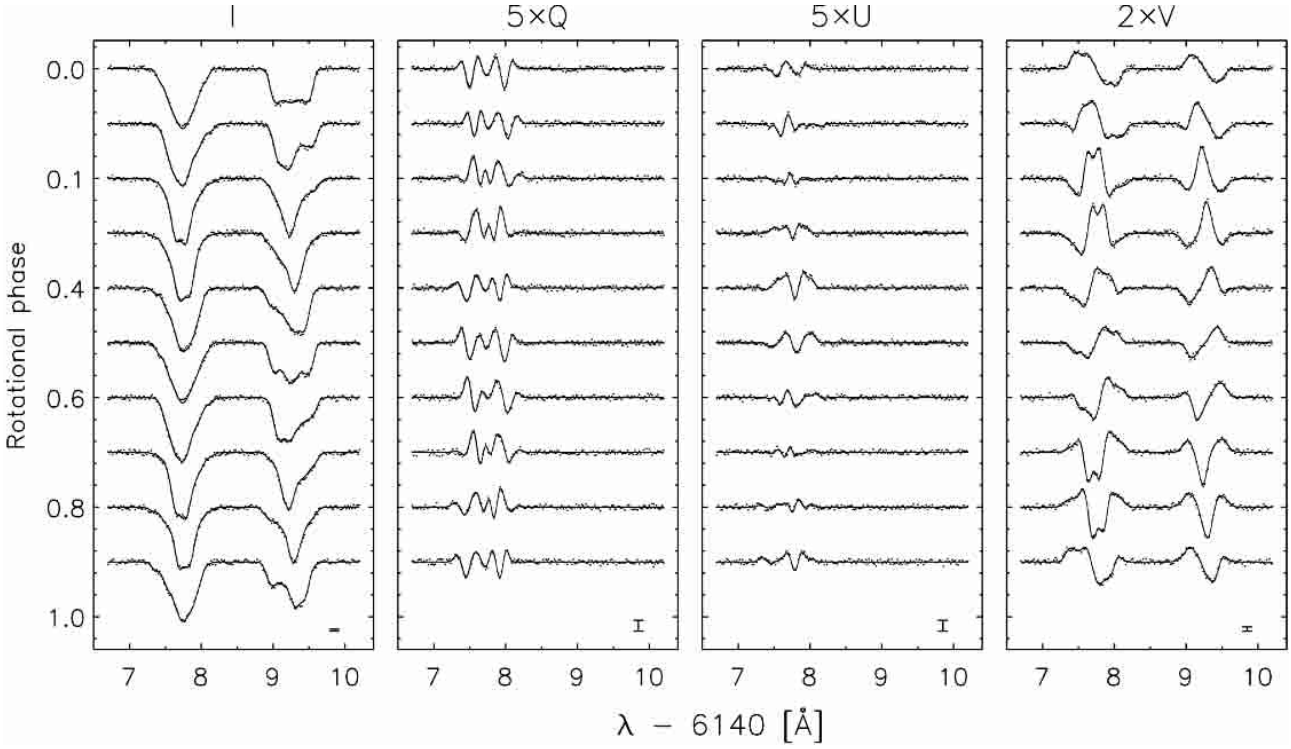

Fig. 7. Synthetic Stokes I, Q, U and V profiles of the Fe II 6147.74 and 6149.26 Å spectral lines calculated for $v \sin i = 10$ km s^{-1} and for the magnetic and abundance distributions shown in Figs. 8 and 9 respectively. Simulated observational data is shown by dots, while the solid lines represent the final fit by the MDI code. The bar at the lower right of each Stokes parameter plot corresponds to 1% of the continuum level of Stokes I.

fine structures in the line profiles of a star with surface abundance inhomogeneities. We found that the quality of abundance reconstruction, in particular determination of the latitudinal position of abundance spots, rapidly deteriorates in the situation when other non-magnetic broadening effects dominate over rotational broadening. This sets a limit of about 3 km s^{-1} for the lowest projected rotational velocity still allowing meaningful abundance imaging with the best possible spectropolarimetric data.

Nevertheless, success of the magnetic imaging of slow rotators is remarkable and very different from the results of conventional abundance or temperature Doppler mapping, which is practically useless for $v \sin i \lesssim 10$ km s^{-1}. Indeed, Fig. 9e demonstrates the results of an attempt to recover the abundance distribution for a non-magnetic star rotating with $v \sin i = 5$ km s^{-1}. Now the code is able to recover only rough longitudinal positions of the abundance spots, but the map is smeared, all latitudinal information is lost and there is a significant general pole-to-equator gradient, which was absent in the true abundance distribution. Comparison of the abundance maps shown in Figs. 9d and e clearly demonstrates that the presence of a strong magnetic field improves abundance recovery for slow rotators (if the abundance image is reconstructed simultaneously with the magnetic map).

Two main effects explain the excellent performance of the MDI technique for slowly rotating stars. First, we use the additional informational content of V, Q and U Stokes profiles, which are strongly modulated due to changing aspect in the course of even the slowest stellar rotation. Second, for the magnetic DI the code uses rotational modulation of the spectra by Doppler *and* Zeeman shifts. Although the latter magnetic effect depends on the (a priori unknown) field distribution, it is as successful in separating wavelength contributions of the individual surface elements to the disk-integrated spectra, as the Doppler effect in rapid rotators. In this sense, if the stellar magnetic field is strong enough, surface structures are resolved by the variable Zeeman shifts, albeit in a much more complicated way than with the rotational Doppler effect. Thus, simultaneously accounting for both the rotational and magnetic contributions to the line profile variability *allows application of the MDI technique to all types of stars with strong global magnetic fields regardless of their* $v \sin i$. The only practical limits are set by the field strength on slow rotators and by the achievable S/N of the spectropolarimetric data collected for rapidly rotating targets.

7. MDI reconstruction for non-optimal orientations of the rotational and magnetic axes

For the dipolar magnetic geometry of the reference test model and non-dipolar magnetic fields of test No. 2 (Sect. 4) we used $i = 60°$ and the magnetic axis perpendicular to the stellar rotational axis ($\beta = 90°$). Such a configuration is ideal for MDI, because both positive and

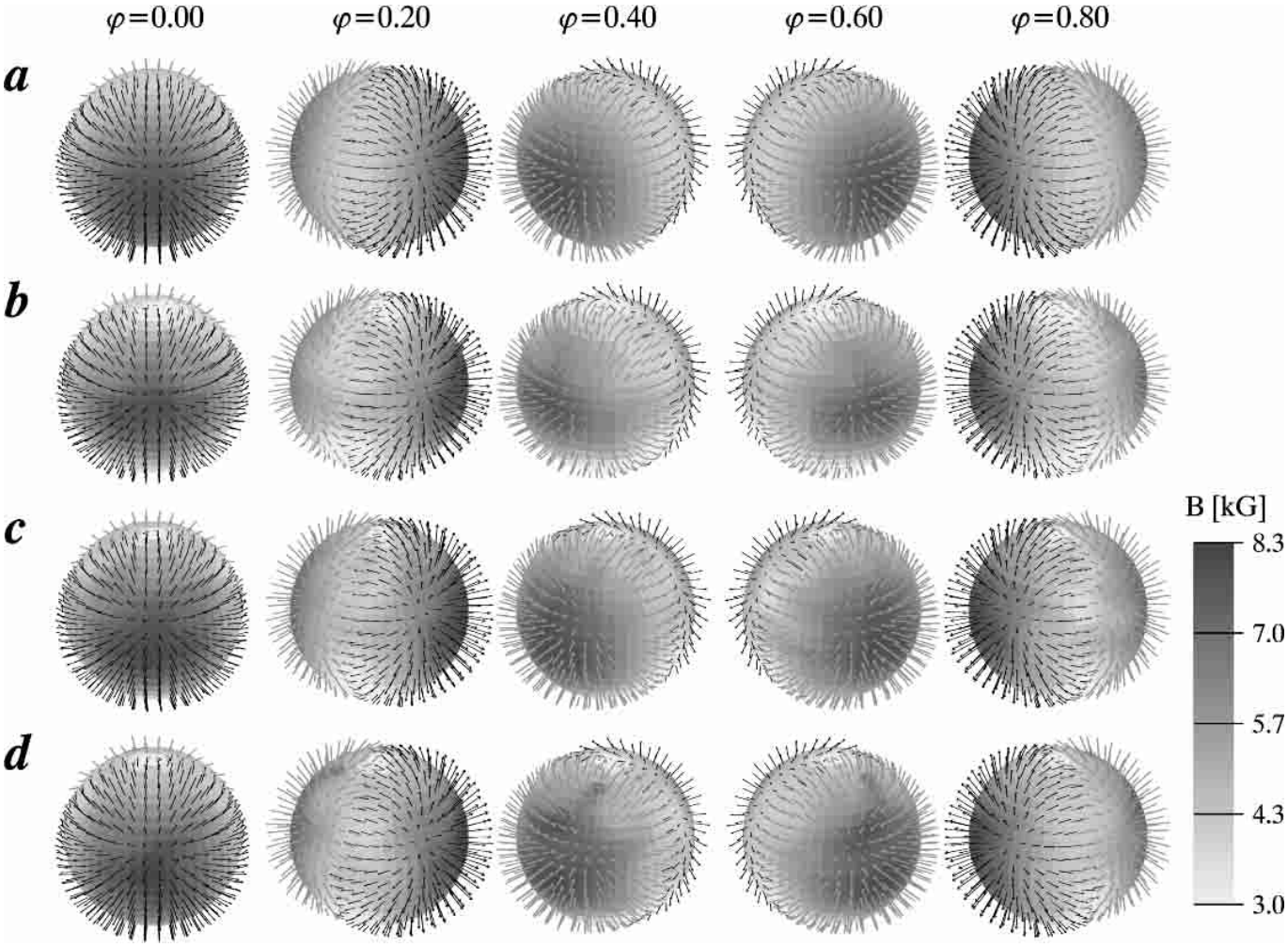

Fig. 8. Magnetic Doppler imaging reconstruction of a dipolar field for different stellar rotational velocities. **a)** is the true map, while **b–d)** show images recovered for stars rotating with $v \sin i$ of 30, 10 and 5 km s^{-1}, respectively.

negative magnetic regions are well sampled during the rotation period and magnetically induced variability of the line profiles is maximal. In reality a significant fraction of early-type magnetic stars do not show polarity reversal of the longitudinal field or viewed close to the rotational pole. In addition, Landstreet & Mathys (2000) found that slowly rotating magnetic stars tend to have generally small β angles. All these effects somewhat reduce variability of the unpolarized line profiles and potentially make field reconstruction from four Stokes parameters more complicated and non-unique.

In order to assess the extent to which the MDI technique is applicable to such non-ideal orientations of the stellar and magnetic axes, we carried out four reconstructions with different combinations of i and β angles, corresponding to the situation when the star is viewed close to the rotational pole ($i = 30°, \beta = 90°$), when β is small or intermediate ($i = 60°, \beta = 30°$ and $\beta = 60°$), and when the star is viewed equator-on ($i = 90°, \beta = 45°$). The last experiment was designed to check if the quality of the MDI reconstruction is hampered by the mirroring effect, which makes surface features above and below the rotational equator completely indistinguishable and precludes application of the conventional DI to stars with $i \simeq 90°$. For all tests we used an 8 kG dipolar field and an homogeneous Fe distribution. As in the majority of other numerical experiments in our paper, the inverse problem was solved for both the magnetic and abundance maps.

Numerical comparison of the true and recovered surface distributions (Table 2) did not show evidence of the degradation of the MDI reconstruction quality for any of the considered combinations of β and i angles. The average abundance and field modulus errors are still below 10%, meridional and azimuthal orientations of the local field vectors are determined with an accuracy of 2–6°, while the strength of the global dipolar component is underestimated by 0.3–0.8 kG. Positions of the magnetic poles on the stellar surface are recovered within 2° in longitude and latitude, and the contribution of a spurious quadrupolar component is below 0.6 kG for all four recovered magnetic maps. Note, that we use the weight function, defined by Eq. (4), for computing the error estimates and multipolar parameters of the magnetic distribution. Thus, the quality parameters listed in Table 2 refer to the field reconstructed

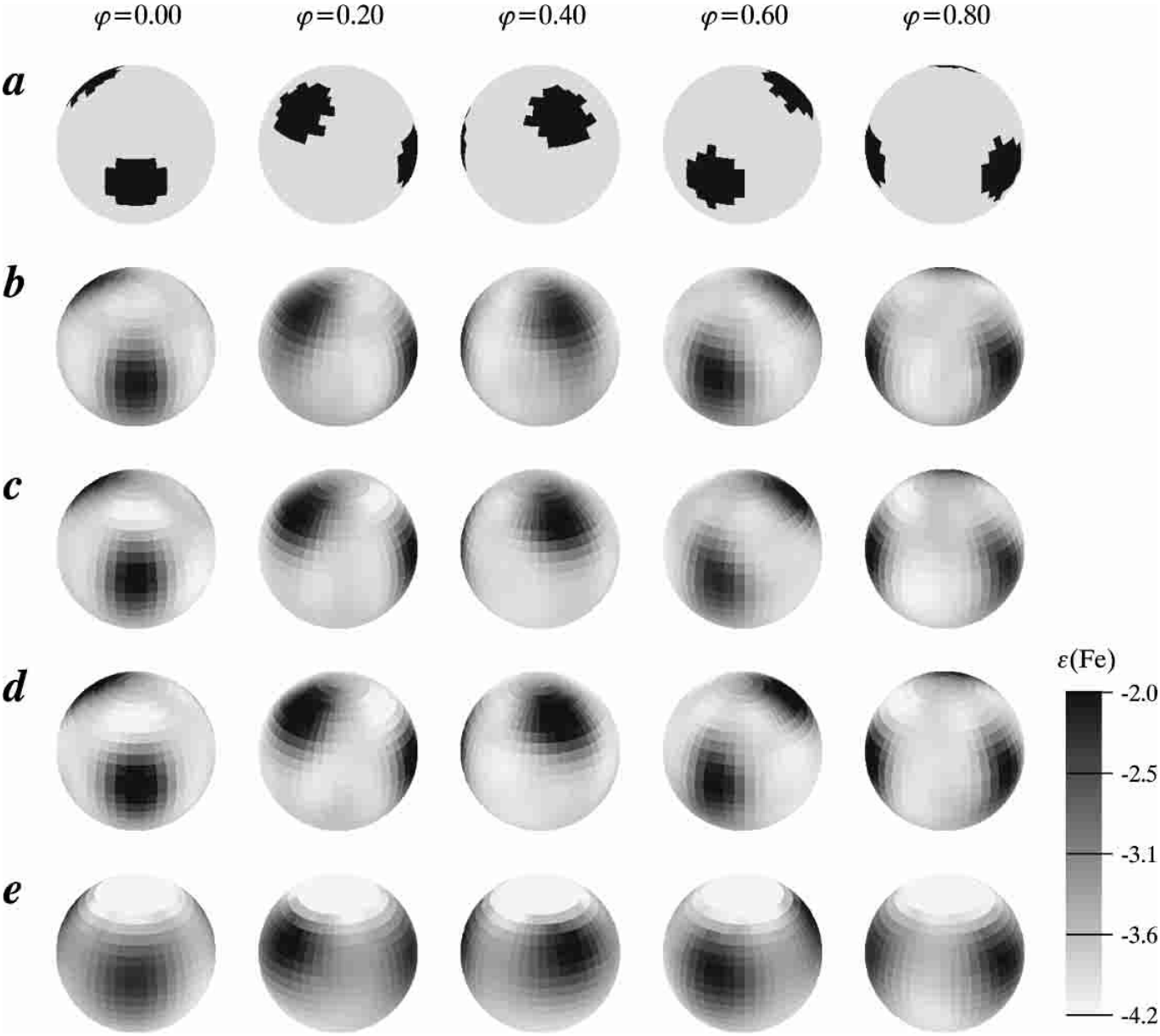

Fig. 9. Abundance distributions recovered simultaneously with the field maps of Fig. 8. In addition to the true abundance map **a)** and Doppler images for $v \sin i = 30$, 10 and 5 km s^{-1} **b–d)**, respectively, results of the reference non-magnetic reconstruction are shown in map **e)**.

only on the visible part of the stellar surface, which is certainly reduced in low inclination tests in comparison with our standard inclination angle $i = 60°$.

We suggest that the good performance of `INVERS10` for all considered orientations of the stellar and magnetic axes is explained by the sensitivity of Stokes Q and U profiles to the transverse component of the stellar magnetic field. Even for very low inclination angles the linear polarization profiles show significant rotational modulation and can be used for modelling. Sensitivity to the transverse field also breaks symmetry for the equator-on test, and, indeed, we did not find any mirroring of the magnetic features for $i = 90°$ and $\beta = 45°$. Numerical experiments confirmed, that *MDI with four Stokes parameters is possible for practically any orientation of the stellar rotation axis and for a wide range of β angles.* At the same time, large βs are certainly more preferable for magnetic imaging, and $i \gtrsim 30°$ is required for the accurate recovery of the abundance part of the stellar surface structure.

8. Sensitivity of MDI to the errors in stellar parameters

Before any DI inversion starts one has to determine a set of the basic stellar parameters $T_{\rm eff}$, $\log g$, $v \sin i$ and i. For MDI with four Stokes parameters it is also necessary to know the azimuth angle Θ of the rotation axis. Moderate errors in the model atmosphere parameters ($T_{\rm eff}$ and $\log g$) usually change only the absolute scale of the reconstructed images, but do not influence the shape of

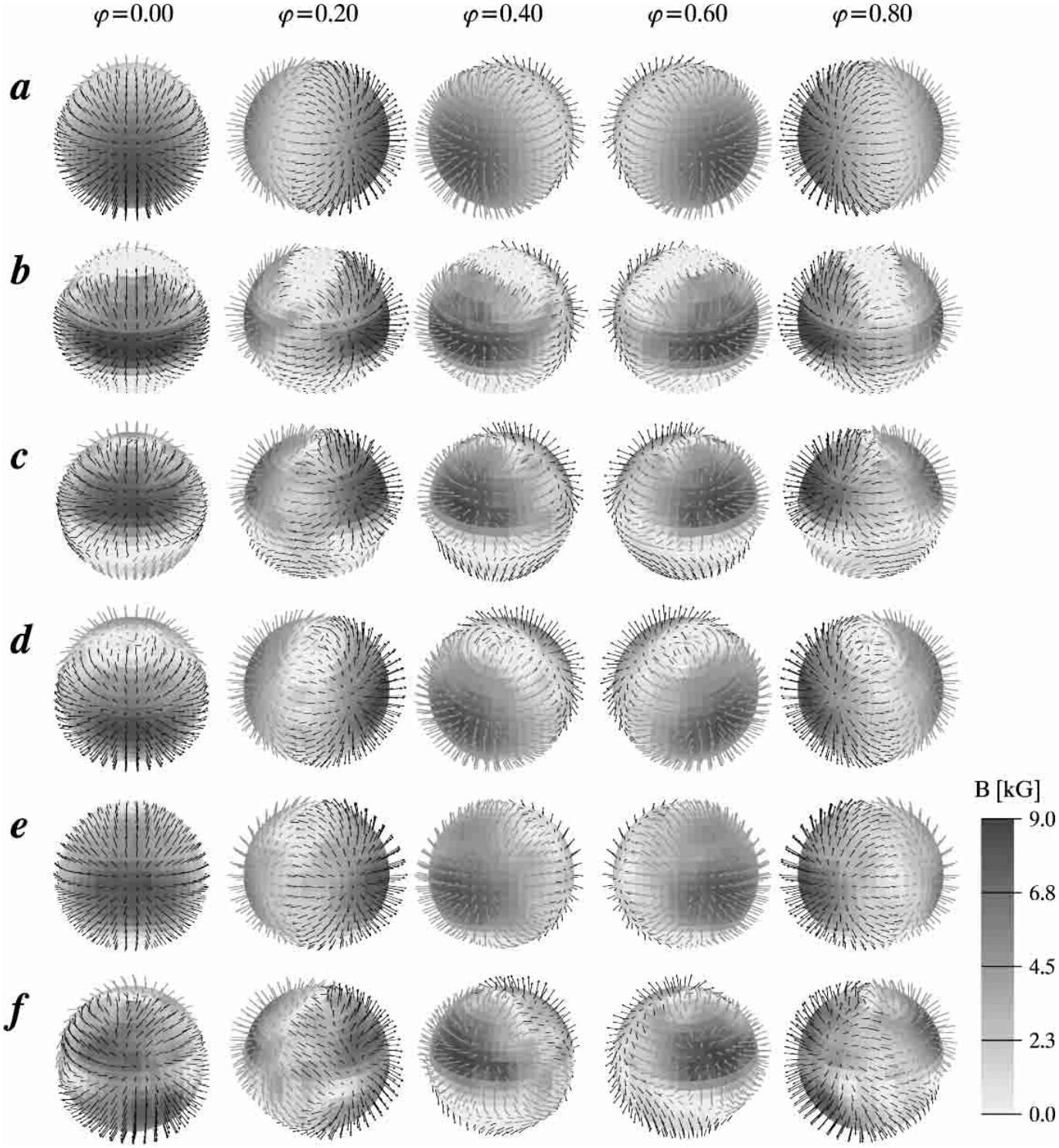

Fig. 10. The influence of the uncertainty in $v \sin i$, i and Θ on the MDI reconstruction. The true magnetic map **a)** is compared with the images obtained assuming $v \sin i = 27$ km s^{-1} **b)** and 33 km s^{-1} **c)**; **d)**, **e)** are reconstructions for $i = 40°$ and $80°$, respectively, while map **f)** illustrates the recovery for $\Theta = 120°$. Simulated observational data was generated with $v \sin i = 30$ km s^{-1}, $i = 60°$ and $\Theta = 90°$.

recovered surface patterns. In a number of abundance and temperature DI simulations (Vogt et al. 1987; Rice et al. 1989) the effects of adopting incorrect values of $v \sin i$ and i were studied. It was found that an incorrectly assumed $v \sin i$ leaves characteristic signatures in a Doppler image. In particular, underestimating $v \sin i$ causes the DI code to produce a band of the enhanced abundance/reduced temperature encircling the star at about the subobserver latitude, while adopting a too large value of the rotational velocity leads to the appearance of an opposite spurious

abundance or temperature pattern. At the same time, conventional DI with Stokes I spectra proved to be relatively insensitive to the errors in the inclination angle i.

Here we examined the influence of incorrect assumptions about $v \sin i$ and orientation of the stellar rotational axis on recovered vector magnetic maps. This is the first such investigation for MDI. Since the response of an abundance distribution to the errors in $v \sin i$ and i is well known, in most of the experiments we recovered only the magnetic distribution and used a fixed homogeneous Fe map. Figure 10 and Table 2 summarize results of the magnetic inversions with wrong stellar parameters.

Similar to conventional DI, adopting an incorrect value of $v \sin i$ significantly affects the quality of the magnetic field recovery. When $v \sin i = 27$ km s^{-1} was used for the analysis of the synthetic Stokes vectors, generated with $v \sin i = 30$ km s^{-1}, `INVERS10` produced a large area of weak field around the intersection of the magnetic equator and rotational pole. In addition, the magnetic distribution lost its symmetry with respect to the magnetic axis and areas of strong field around magnetic poles were stretched in the longitudinal and compressed in the latitudinal direction. On the other hand, using $v \sin i = 33$ km s^{-1} mostly hampers the quality of the field recovery in intermediate and low latitude regions. Figure 10c shows that in this case a band of weak field appears at and below the rotational equator and field polarity is recovered incorrectly for $\rho \lesssim -30°$. In general underestimating $v \sin i$ by 3 km s^{-1} produces lower average errors in recovered field strength and orientation than adopting a too high value of the rotational velocity. The expansion of the final magnetic maps into spherical harmonics confirms this conclusion: a global dipolar field with the polar strength $B_{\rm d} = 7.0$ kG and a negligible quadrupolar contribution fits the magnetic image recovered with $v \sin i = 27$ km s^{-1}, while overestimating rotational velocity gives rise to a quadrupolar component which is stronger than the dipole contribution ($B_{\rm d} = 4.5$ kG, $B_{\rm q} = 5.0$ kG).

An incorrect estimate of $v \sin i$ for slow rotators produces very similar effects. However, as the importance of rotational broadening decreases, larger relative errors of the $v \sin i$ determination become acceptable for spectra of a given resolution. For example, for a star rotating with $v \sin i = 5$ km s^{-1} it is necessary to derive rotational velocity with an accuracy of $\approx$20% or better, compared with a $\approx$10% error margin for a star with a projected rotational velocity of 30 km s^{-1}.

Magnetic distributions reconstructed with incorrect values of $v \sin i$ do not fit observational data to the same level that was achieved in MDI with the correct $v \sin i$. The most pronounced effect was found for Stokes I, for which the final deviations increased by a factor of 2. Given an incorrect estimate of the rotational velocity, `INVERS10` is unable to produce a misleading solution which gives low χ^2. Therefore, the optimal rotational velocity can be determined in the MDI by comparing the final χ^2 for the inversions with various values of $v \sin i$.

In the next two numerical experiments we analysed the inclination effect in MDI. Figures 10d and e illustrate these tests and show that the magnetic imaging is not sensitive to inclination errors as large as 20°. Neither the χ^2 of the final fit to observational data, nor the average errors showed a tendency to increase when $i = 40°$ or $i = 80°$ was adopted instead of the true inclination angle $i = 60°$. The strength of the global dipolar field was underestimated by 0.6 kG, while the contribution of a spurious quadrupolar magnetic component and errors in the orientation of the magnetic axis were found to be below 0.8 kG and 0.5°, respectively. These figures do not differ significantly from the reconstruction results obtained for the reference test model. Thus, using a precise value of i is not crucial for MDI. On the other hand, this means that magnetic imaging by itself cannot provide an accurate estimate of this stellar parameter.

The impact of an incorrect assumption of the azimuth angle Θ is somewhat similar to the effect of adopting an incorrect $v \sin i$. Figure 10f demonstrates that an error of 30° in Θ leads to the strong "twisting" distortions of the recovered magnetic distribution and increases typical errors of the local field strength and orientation by 50–100%. The strength of the global field is below the true value by 2.2 kG, and a false quadrupole contribution with $B_{\rm q} = 3.0$ kG appears in the recovered magnetic image. However, `INVERS10` did not achieve an acceptable fit to the Stokes profiles with this magnetic model. The final χ^2 for all four Stokes parameters was 1.5–2 times the deviation for the imaging with the correct orientation of the stellar rotational axis. Sensitivity of the MDI to the azimuth angle suggests that Θ should be determined with an accuracy better than 10° for the successful magnetic reconstruction. The required accuracy can be obtained by minimizing χ^2, similar to the procedure outlined above for the rotational velocity. For some magnetic CP stars good initial estimates of Θ are available from the modelling of the broadband linear polarization (Leroy et al. 1996).

The conclusions of this section will not change significantly if the MDI recovery is carried out simultaneously for abundance and magnetic distributions. In general the quality of the recovered magnetic maps and the fit to observational data remains the same if the iron distribution is allowed to vary in the tests with an incorrect assumption of the inclination. In the similar experiments with an incorrect $v \sin i$ and azimuth angle, χ^2 and recovery errors slightly decrease but `INVERS10` achieves this improvement by producing spurious pole-to-equator gradients in the abundance maps. Interestingly enough, with the adopted magnetic geometry an overestimate of $v \sin i$ leads to the same distortion in the abundance map that is caused by using the wrong Θ: `INVERS10` reconstructs a large polar spot with the enhanced iron abundance, while Fe concentration on the rotational equator is underestimated.

Numerical experiments demonstrate that `INVERS10` *is remarkably robust with respect to the errors in* $v \sin i$ *and orientation of the rotational axis.* MDI is either very

weakly sensitive to the adopted parameter (i), or fails to find an appropriate fit to the observational data if wrong values are used for the parameters to which sensitivity is high ($v \sin i$ and Θ). This makes it possible to use in the magnetic imaging (rather crude) estimate of the inclination from the rotational period, $v \sin i$ and stellar radius and adjust the rotational velocity and the azimuth angle by minimizing residuals of the fit to the observed Stokes profiles.

9. MDI sensitivity to the quality of observational data

It is of great interest to investigate the sensitivity of the magnetic images derived by `INVERS10` to various parameters of the spectropolarimetric observational data. In the real world one often has to deal with noisy spectra having a sparse or incomplete phase coverage. Current observational restrictions are even more severe for Stokes Q and U profiles, which have been systematically measured with only a poor S/N and relatively low spectral resolution of $R \approx 35\,000$ (Wade et al. 2000a).

To get an estimate of the magnetic image degradation with decreasing quality of Stokes I, Q, U and V profiles we recovered the standard dipolar magnetic distribution using low-resolution ($R = 20\,000$) Stokes vectors, observational data consisting of 5 equidistant phases, spectra with a phase gap of 0.4 around phase 0.0 and observational material with a poor S/N (60 for Stokes I, 90 for Stokes V and 240 for linear polarization profiles). A complex iron abundance distribution, similar to the one used in test No. 4 (Sect. 6), was recovered simultaneously with the magnetic images.

The results of the tests are shown in Fig. 11. Decreasing the spectral resolution does not produce strong distortions of the magnetic map. The main features of the dipolar field are well-defined, but some contrast is lost in the abundance image and the high-latitude spot of iron overabundance is stretched in the latitudinal direction. In addition, instrumental smearing of Stokes parameters allows the MDI code to fit observations with a weaker field distribution. This leads to the underestimate of the dipole strength by 1.1 kG – almost twice the value typical for $R = 100\,000$.

The effects of a poor phase coverage and reduced S/N are all rather similar. Since less information is available for the magnetic imaging, the MDI code looses detailed resolution of the stellar surface, producing images with more irregularities. Major magnetic structures are properly recovered only at the subobserver latitude of the star, while the field strength is generally underestimated around the rotational pole and below the stellar equator. `INVERS10` is also not very successful in identifying the global dipolar structure in the magnetic topology: $B_{\rm d}$ is underestimated by 1.4–2.2 kG and a spurious quadrupole contribution with $B_{\rm q} = 1.6$–2.6 kG is evident in the recovered magnetic maps. However, our MDI code still does a good job in reconstructing polarity of the magnetic distribution and recovers the orientation of the magnetic axis within 4° of the true $\beta_{\rm d}$ and $\gamma_{\rm d}$. Abundance maps are reproduced fairly well in the experiments with a poor phase coverage and reduced S/N. The only exception was the test with incomplete phase coverage, when the code lost most of the information about the spot, which passes close to the line-of-sight in the middle of the phase gap.

From the numerical tests of this section it is possible to formulate some practical quality requirements for the observational data used in MDI. Since magnetic reconstruction is more sensitive to phase coverage and S/N ratio than abundance maps, *it is necessary to obtain a fair coverage of the rotational period ($\geq$10 phases with the largest phase gap not exceeding 0.15–0.20). Signal-to-noise ratio should preferrably be above 250–300 for Stokes I and allow detection of the polarization signal at $\geq 3\sigma$ level for most of the rotational phases in Stokes Q, U and V parameters.* These quality parameters translate to S/N ratios of 700–1000 for MDI with four Stokes parameters and moderately strong or medium strength magnetically sensitive spectral lines. Such noise levels can be achieved for stars brighter than 8–9 magnitude in reasonable exposure times ($\lesssim$1 hour) with 3–4-meter-class telescopes equipped with existing instruments, such as a polarimeter combined with the UCL Echelle Spectrograph at the Anglo-Australian Telescope (Donati et al. 1997) or next generation spectropolarimeters, similar to the ongoing ESPaDOnS project for the Canada-France-Hawaii Telescope (Donati et al. 1998). As for the spectral resolution, *a full four Stokes parameter inversion requires data with $R \geq 50\,000$ for moderate rotators and R close to 10^5 for slowly rotating CP stars.*

10. MDI with Stokes I and V parameters

In the preceding sections we demonstrated that reliable MDI recovery of an arbitrary magnetic field without any assumptions about the field geometry is possible with high-quality spectropolarimetric data in four Stokes parameters. Such complete Stokes vector datasets exist for only a limited number of magnetic CP stars (Wade et al. 2000a), and resolution and noise characteristics of these spectra preclude their direct use in magnetic DI. At the same time there exist several high-resolution échelle spectrographs, capable of measuring circular polarization profiles with a high accuracy over wide spectral regions. In fact, parameter optimization of the multipolar magnetic models, carried out in previous MDI studies of CP stars (Piskunov 1985; Khokhlova et al. 2000), never extended beyond fitting Stokes I and V profiles. Thus, it is important to investigate the performance of `INVERS10` in the problem of magnetic and abundance recovery without linear polarization observations.

As we explained in Paper I, an inverse problem regularized with the conventional Tikhonov functional becomes less well-defined in this case. As a result reconstruction of the magnetic structures is more difficult, especially when one tries to recover the magnetic image

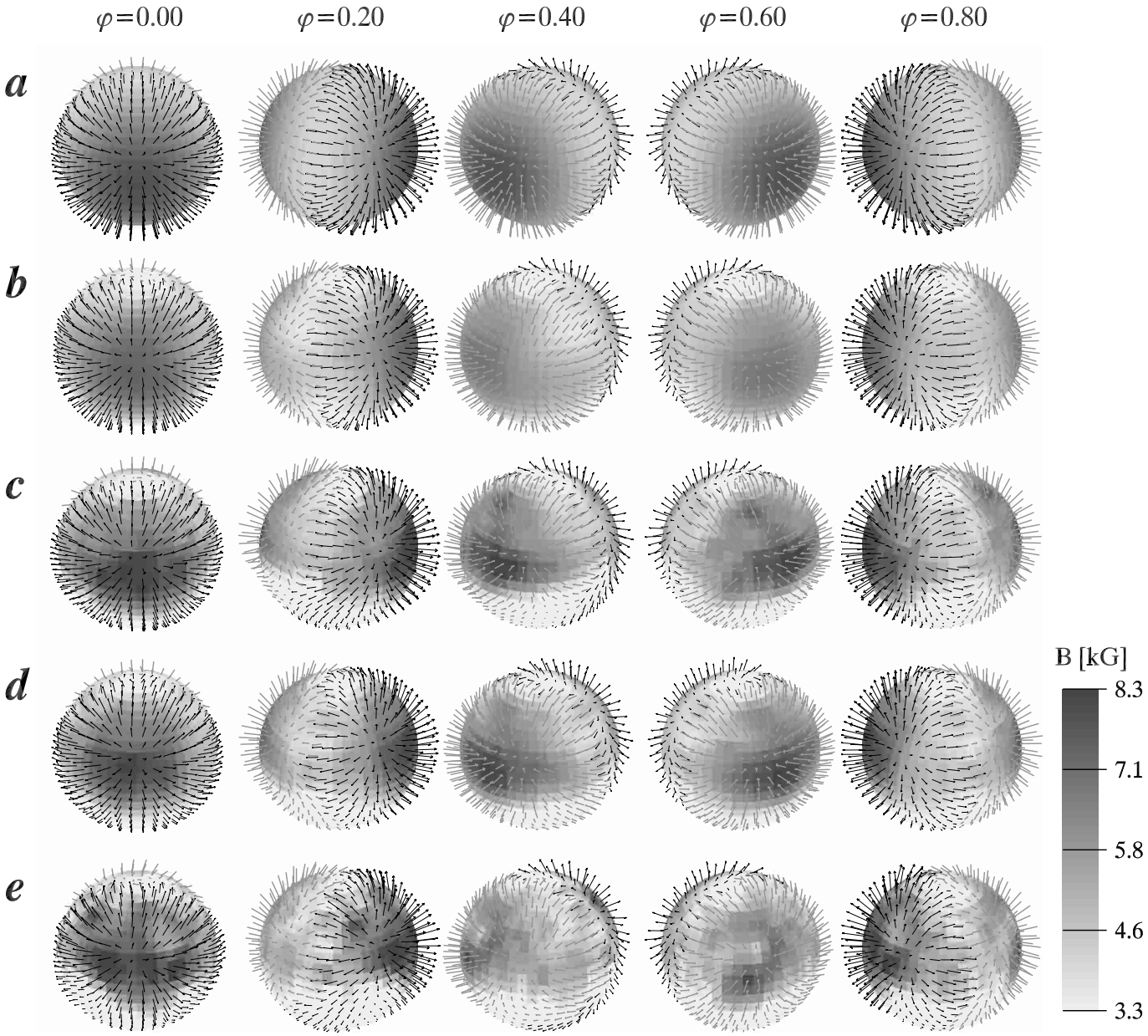

Fig. 11. The influence of the quality of observational data on the MDI reconstruction. The true magnetic map **a)** is compared with the magnetic images obtained from a Stokes $IQUV$ dataset with the reduced spectral resolution $R = 20\,000$ **b)**, phase coverage consisting of only 5 equidistant rotational phases **c)**, spectral data with a gap of 0.4 in phase coverage **d)** and from the Stokes parameters with reduced S/N **e)**.

using different non-zero initial guesses. Similar to the stability test, described in Sect. 3, we attempted to recover an 8 kG dipolar field using simulated observations in Stokes I and V parameters and adopting a zero field, an homogeneous radial field and the true dipolar field, rotated by 90° in longitude, as initial guesses for the magnetic distribution. Table 3 summarizes results of these experiments and confirms the suspicion that incomplete polarization data leads to the degradation of the magnetic image. Typical errors of the field strength and azimuthal direction recovery increase substantially as compared to the imaging with four Stokes parameters. The strongest effect is observed for the meridional direction of the local field vectors, which systematically deviates from the true orientation by 10–30°. In addition, most of the field structure is recovered only near the subobserver latitude and around the visible rotational pole, while at the stellar equator and below field strength is significantly underestimated and no information about the field orientation could be obtained.

Unsuccessful magnetic recovery in the considered IV imaging tests is caused by the intrinsic limitations of the informational content of an incomplete Stokes parameter dataset, but not by an incorrect fitting of the observations. As pointed out by Brown et al. (1991), the effective limb darkening is stronger for Stokes V parameter than for Stokes I. Therefore, at each rotational phase circular

Table 3. Numerical tests of the MDI reconstruction using Stokes I and V parameters. Magnetic distributions adopted for the tests consisted of the dipolar field D with parameters (8, 90°, 0°) or combination of the dipole and axisymmetric quadrupole $D+Q$ with parameters (8, 90°, 0°)+(8, 90°, 0°). Parameterization of the magnetic multipoles is explained in the caption of Table 2, while calculation of the error estimates $\delta\varepsilon$, δB, $\delta\rho$ and $\delta\eta$ is detailed in Sect. 2. The last two columns show the strengths of the magnetic dipole $B_{\rm d}^{\rm rec}$ and non-axisymmetric quadrupole $B_{\rm q}^{\rm rec}$ derived by the second-order multipolar expansion of the reconstructed magnetic maps.

Test No.	Surface distributions ε(Fe)	magnetic field	Regularization functional	Initial guess for magnetic field	$\delta\varepsilon$ (%)	δB (%)	$\delta\rho$ (°)	$\delta\eta$ (°)	$B_{\rm d}^{\rm rec}$ (kG)	$B_{\rm q}^{\rm rec}$ (kG)
1	*Reconstruction from the different initial magnetic distributions*									
	no spots	D	Tikhonov	zero field	9.6	15.4	19.2	2.3	6.32	0.24
	no spots	D	multipolar	zero field	5.2	4.8	1.6	1.1	7.68	0.48
	no spots	D	Tikhonov	radial field	10.7	9.3	33.6	10.0	6.00	2.32
	no spots	D	multipolar	radial field	7.7	8.0	7.2	2.1	7.52	1.52
	no spots	D	Tikhonov	rotated dipole	11.4	15.5	24.9	3.0	6.16	0.56
	no spots	D	multipolar	rotated dipole	5.3	3.2	2.6	1.2	7.92	0.48
2	*Reconstruction of the complex abundance distribution and dipolar magnetic map*									
	3 spots	D	Tikhonov	zero field	31.8	26.2	23.2	5.1	5.28	1.76
	3 spots	D	multipolar	zero field	26.3	12.2	8.0	2.3	7.12	1.44
3	*Complex global magnetic distribution*									
	no spots	$D+Q$	Tikhonov	zero field	15.0	14.3	35.8	4.8	7.09	5.60
	no spots	$D+Q$	multipolar	zero field	8.6	10.3	6.5	3.1	7.20	8.32

polarization is dominated by the contribution from magnetic regions close to the disk center, and during the whole rotational period it remains relatively insensitive to the field structures far from the subobserver latitude.

The only way to correct the loss of information about the transverse field component is to use an additional, external restriction for the stellar magnetic topology. Superposition of low-order multipoles was shown to be a good approximation for the field distributions on the magnetic CP stars and magnetic white dwarfs. Thus, we suggest to restrict the family of possible solutions of the IV imaging problem by demanding its proximity to a combination of magnetic multipoles. This restriction was implemented in the form of a novel multipolar regularization method, which was discussed in Sect. 2.7 of Paper I. It was demonstrated that this regularization scheme is consistent with the global multipolar structure of the fields on early-type stars, unlike the conventional Tikhonov or Maximum Entropy regularizations which fail when a problem becomes more dependent on the regularization algorithm, as in the case of the MDI with Stokes I and V profiles.

Application of the second-order multipolar regularization to the IV recovery from different initial guesses confirmed the efficiency of the code. For all three test cases `INVERS10` converged to the magnetic distributions, which deviated from the true maps by typically 5–8% in the field strength and 2–7° in the meridional orientation of the local field vectors. The comparison of the multipolar expansion parameters indicated that the multipolar regularization also improved the recovery of a global dipolar magnetic pattern. Analysis of the final `INVERS10` magnetic maps showed that the dominant component of the magnetic topology is a dipole with $B_{\rm d}=7.5$–7.9 kG, while in the IV imaging with the Tikhonov regularization $B_{\rm d}$ was typically underestimated by 1.7–2.0 kG.

A new regularization method was further tested in a more complicated IV imaging simulation, which included simultaneous recovery of an 8 kG dipolar field and a complex Fe distribution. Figure 12 compares the magnetic images and the abundance maps obtained with the Tikhonov and the multipolar functionals. The corresponding true distributions of Fe and magnetic field are displayed in Figs. 9a and 8a. Reconstruction with the conventional regularization scheme showed all degradation signs described above, but application of the multipolar regularization of the solution allowed accurate recovery of the main magnetic features to be achieved. In particular, much better results were obtained for the stellar surface regions at and below the rotational equator. Furthermore, the abundance map recovered in the experiment with the multipolar functional has slightly better contrast than the distribution derived with the Tikhonov magnetic regularization. This improvement reflects some crosstalk between the abundance and magnetic maps, since Fe images were regularized with the Tikhonov functional in both reconstructions. But even grossly inadequate Stokes IV/Tikhonov regularization field recovery (Fig. 12c) leads to only a mild homogeneous smearing of the abundance map (Fig. 12a), and not to the appearence of spurious surface features.

In the last set of simulations multipolar regularization was tested in the IV imaging of a complex global magnetic field. The magnetic model that we adopted was identical to one of the magnetic topologies reconstructed in test No. 2 and consisted of an aligned dipole and axisymmetric quadrupole ($B_{\rm d}=B_{\rm q}=8$ kG, $\beta_{\rm d}=\beta_{\rm q}=90°$, $\gamma_{\rm d}=\gamma_{\rm q}=0°$). No Fe spots were introduced in the abundance map, but the iron distribution was treated as a free parameter during reconstruction. Figure 13 illustrates the

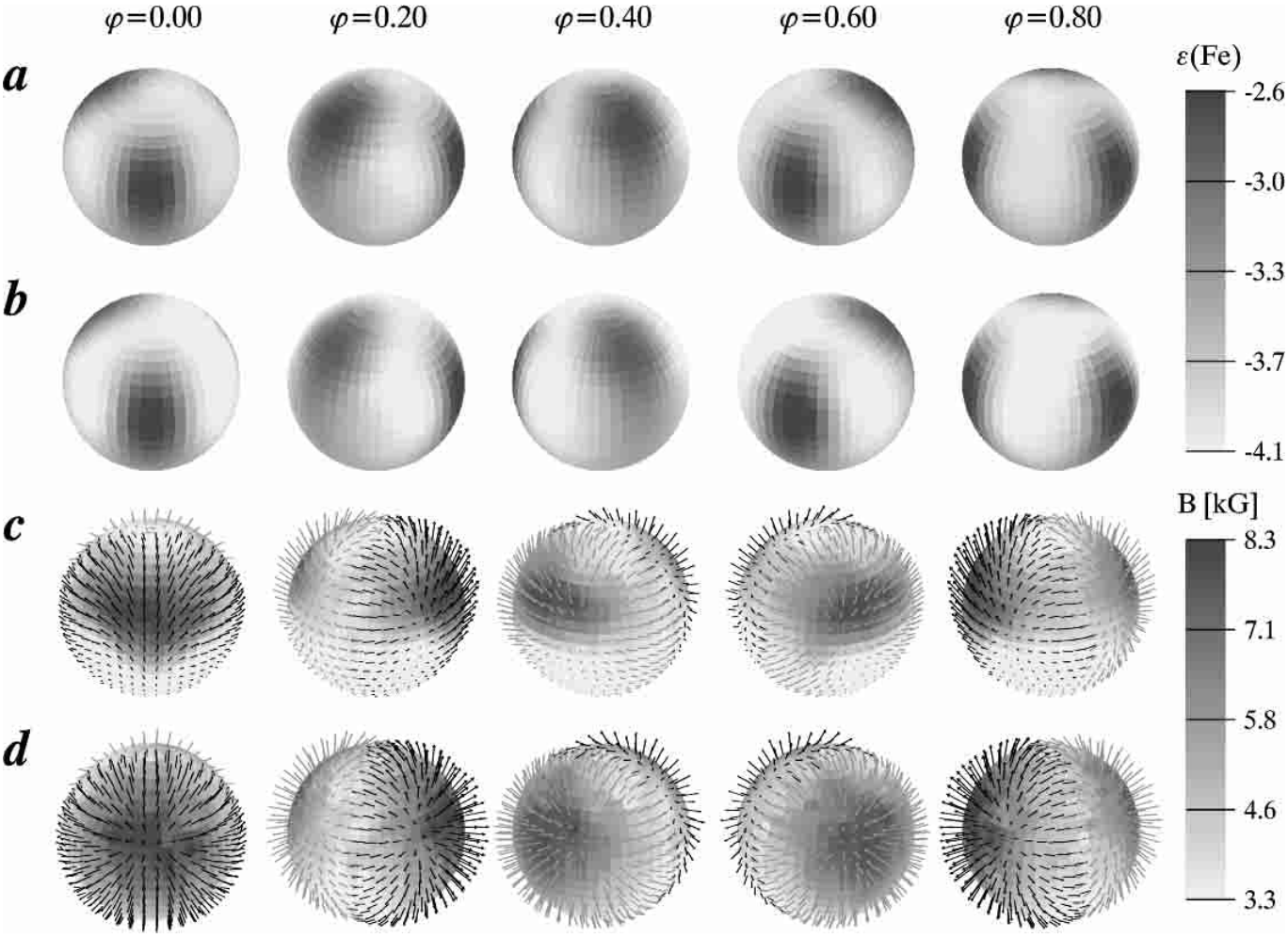

Fig. 12. Simultaneous recovery of the abundance and magnetic dipole distributions of Figs. 9 and 8 from Stokes I and V data. **a)** and **c)** are the images reconstructed with the Tikhonov regularization, while **b)** and **d)** are images regularized with the multipolar functional.

recovered magnetic images and compares the true map with the images regularized by the Tikhonov and multipolar methods. Once again, the magnetic map based on the Tikhonov regularization shows characteristic crosstalk from the radial to meridional field component and failure to recover field in the low-latitude regions. Much better results in terms of the average errors δB, $\delta\rho$ and $\delta\eta$ were achieved with the multipolar regularization. The global field structure was also better resolved in the latter experiment. It converged to $B_{\rm d} = 7.2$ kG, $\beta_{\rm d} = 91°$ and $B_{\rm q} = 8.4$ kG, $\beta_{\rm q} = 85°$, while the corresponding parameters of the imaging with the Tikhonov method were $B_{\rm d} = 7.1$ kG, $\beta_{\rm d} = 116°$ and $B_{\rm q} = 5.6$ kG, $\beta_{\rm q} = 100°$.

Simulations carried out in this section show that *much of the information about the abundance distribution and magnetic field structure can be successfully extracted from the time series of Stokes I and V parameters* using MDI based on the multipolar regularization. However, IV imaging with the multipolar regularization could hardly match all capabilities of the MDI with four Stokes parameters. It remains somewhat biased due to its intrinsic preference to low-order multipolar fields. In addition, we expect that the performance of this method could not compete with four Stokes parameter imaging for combinations of stellar parameters, significantly departing from the optimal MDI configuration (large i, β and moderate $v \sin i$) used in our IV tests.

11. Conclusions

We have presented an extensive set of numerical simulations of magnetic Doppler Imaging reconstruction of stellar magnetic fields using high-resolution spectropolarimetric data. These experiments allowed us to conduct a thorough testing of our new MDI code `INVERS10` and examine the performance of the MDI method under realistic conditions. Results of our tests can be briefly summarized as follows.

– We showed that high-resolution four Stokes parameter time series contain enough information for the accurate and self-consistent magnetic DI reconstruction of the magnetic field geometry and abundance distribution. Simultaneous magnetic and abundance inversion

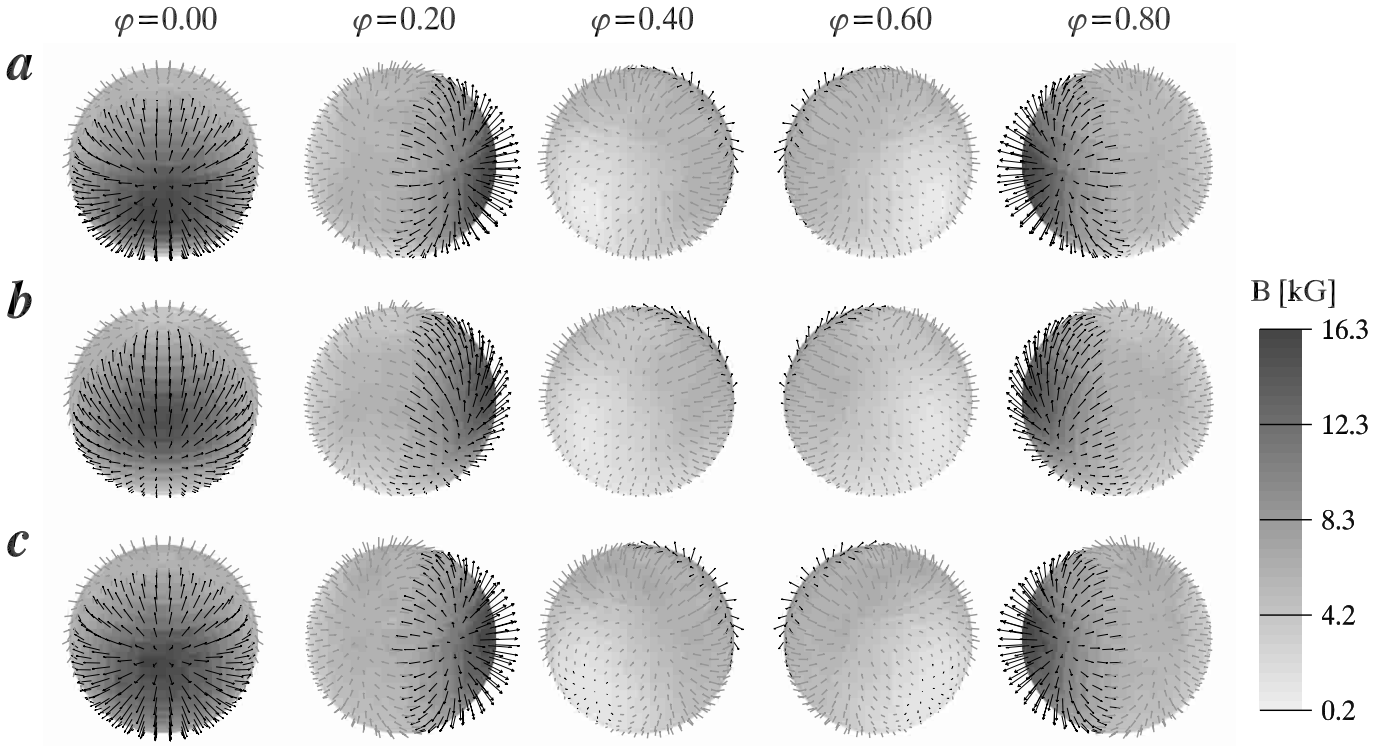

Fig. 13. Recovery of the complex global magnetic distribution using Stokes I and V spectra. The true magnetic map **a)** (combination of the aligned dipole and axisymmetric quadrupole) is compared with the field recovered using the Tikhonov **b)** and multipolar **c)** functionals.

is stable, insensitive to the initial guess and does not require any a priori assumptions about the global stellar magnetic topology.

- Our MDI code is not restricted to the reconstruction of the simpliest dipolar magnetic geometries. We believe that the code can be successfully applied to the imaging of global stellar magnetic fields and abundance distributions of an arbitrary complexity.
- Unlike conventional abundance and temperature Doppler mapping, an MDI code extracts the information about the stellar surface structures not only from the rotational Doppler shifts, but also from the rotational modulation of the orientation and strength of the magnetic field. This makes it possible to image the magnetic and abundance structures on the surfaces of very slowly rotating stars.
- DI based on observations in four Stokes parameters is possible for a wide range of orientations of the stellar and magnetic axes. Furthermore, sensitivity of the linear polarization measurements to the transverse field component allows useful information about magnetic topology to be extracted even in the nearly pole-on and equator-on orientations, where conventional scalar DI is useless.
- Tests of the sensitivity of our code to errors in the input stellar parameters showed that successful magnetic inversion requires accurate input values of the rotational velocity $v \sin i$ and the azimuth angle of the rotational axis Θ. On the other hand, `INVERS10` is weakly sensitive to moderate errors in the inclination of the rotational axis i. Furthermore, given incorrect assumptions of stellar parameters, the MDI code is not capable of finding a spurious solution that provides a good fit to the observational data.
- We carried out several numerical experiments designed to evaluate the sensitivity of the MDI code to the quality of observational data. The results of these tests suggest that in order to be useful for magnetic DI, spectra in four Stokes parameters must have resolution $R \geq 50\,000$, an even coverage of the stellar rotational period with at least 10 phases, have a S/N above 250 for Stokes I and allow reliable detection of the polarization signal in other Stokes parameters. Numerical experiments confirmed that observational data required for the full application of `INVERS10` can be obtained with existing spectropolarimeters or instruments that will become available in the near future.
- We concluded numerical experiments with several tests of the magnetic reconstruction using incomplete Stokes parameter datasets containing only Stokes I and V profiles. We found that IV imaging of global stellar magnetic fields is possible with the multipolar regularization method, which restricts the family of possible solutions of the MDI problem by demanding its proximity to a multipolar field geometry.

The results of the tests presented in this paper confirm the capabilities of `INVERS10` and allow us to proceed with the applications to real stars which we plan to present in the next paper of this series.

Acknowledgements. This work was supported by the Swedish National Research Council. We would also like to thank the Knut and Alice Wallenberg Foundation for contributing the state-of-the-art computing facilities at the Institute of Astronomy and Space Physics in Uppsala. We thank the referee S. Bagnulo for constructive remarks which contributed to the improvement of our paper.

References

Bagnulo, S., Landolfi, M., & Landi Degl'Innocenti, M. 1999, A&A, 343, 865

Brown, S. F., Donati, J.-F., Rees, D. E., & Semel, M. 1991, A&A, 250, 463

Donati, J.-F. 2001, in First International Workshop on Astro-Tomography, ed. H. Boffin, D. Steeghs, & J. Cuypers (Springer, Berlin), 207

Donati, J.-F., & Brown, S. F. 1997, A&A, 326, 1135

Donati, J.-F., Semel, M., Carter, B. D., Rees, D. E., & Cameron, A. C. 1997, MNRAS, 291, 658

Donati, J.-F., Catala, C., & Landstreet, J. D. 1998, in Proceedings of the fifth CFHT users' meeting, ed. P. Martin, & S. Rucinski, 50

Khokhlova, V. L., Vasilchenko, D. V., Stepanov, V. V., & Romanyuk, I. I. 2000, Sov. Astron. Lett., 26, 177

Kupka, F., Piskunov, N., Ryabchikova, T. A., Stempels, H. C., & Weiss, W. W. 1999, A&AS, 138, 119

Kurucz, R. 1993, CD-ROM No. 13, Smithsonian Astrophys. Obs.

Landolfi, M., Bagnulo, S., & Landi Degl'Innocenti, M. 1998, A&A, 338, 111

Landstreet, J. D., & Mathys, G. 2000, A&A, 359, 213

Leroy, J.-L., Landolfi, M., & Landi Degl'Innocenti, E. 1996, A&A, 311, 513

Mathys, G. 1990, A&A, 232, 151

Mathys, G., Hubrig, S., Landstreet, J. D., Lanz, T., & Manfroid, J. 1997, A&AS, 123, 353

Piskunov, N. E. 1985, Sov. Astron. Lett., 10, 449

Piskunov, N. E., & Wehlau, W. H. 1990, A&A, 233, 497

Piskunov, N., & Kochukhov, O. 2002, A&A, 381, 736

Rice, J. B., Wehlau, W. H., & Khokhlova, V. L. 1989, A&A, 208, 179

Rice, J. B., & Strassmeier, K. G. 2000, A&AS, 147, 151

Sobelman, I. I. 1979, Atomic Spectra and Radiaitve Transitions, Springer Series in Chemical Physics, vol. 1 (Springer-Verlag, Berlin)

Vogt, S. S., Penrod, G. D., & Hatzes, A. P. 1987, ApJ, 321, 496

Wade, G. A., Donati, J.-F., Landstreet, J. D., & Shorlin, S. L. S. 2000a, MNRAS, 313, 823

Wade, G. A., Donati, J.-F., & Landstreet, J. D. 2000b, New Astron., 5, 455

Wickramasinghe, D. T., & Ferrario, L. 2000, PASP, 112, 873